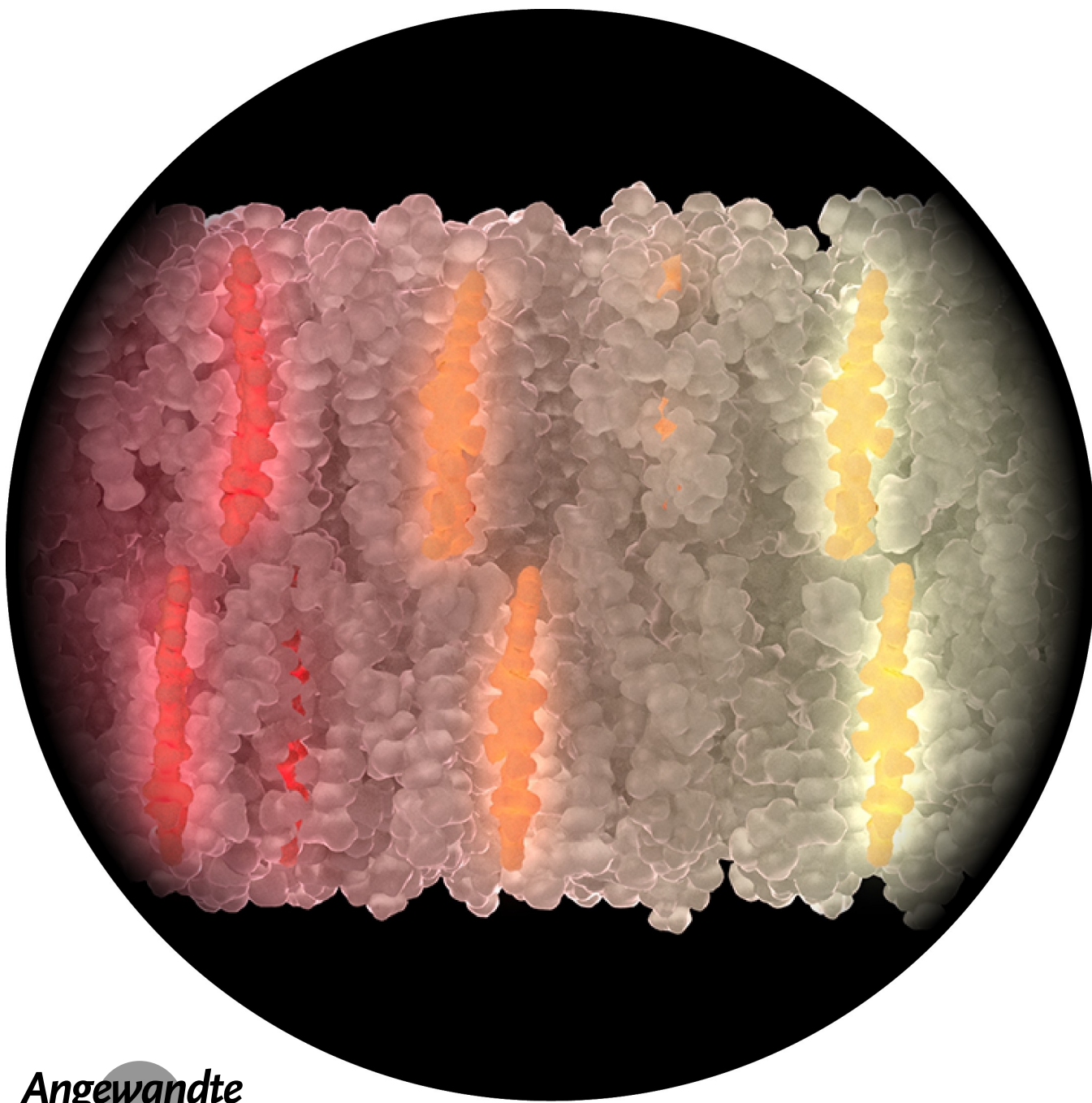


Fluorescent Flippers: Small-Molecule Probes to Image Membrane Tension in Living Systems

Xiao-Xiao Chen, Felix Bayard, Nerea Gonzalez-Sanchis, Khurnia Krisna Puji Pamungkas, Naomi Sakai, and Stefan Matile*



Abstract: Flipper probes have been introduced as small molecule fluorophores to image physical forces, that is, membrane tension in living systems. Their emergence over one decade is described, from evolution in design and synthesis to spectroscopic properties. Responsiveness to physical compression in equilibrium at the ground state is identified as the ideal origin of mechanosensitivity to image membrane tension in living cells. A rich collection of flippers is described to deliver and release in any subcellular membrane of interest in a leaflet-specific manner. Chalcogen-bonding cascade switching and dynamic covalent flippers are developed for super-resolution imaging and dual-sensing of membrane compression and hydration. Availability and broad use in the community validate flipper probes as a fine example of the power of translational supramolecular chemistry, moving from fundamental principles to success on the market.

1. Introduction

Newton's apple, which presumably fell in his garden during the Great Plague confinement in 1665, stands as the perfect illustration of why detecting physical forces is so challenging. This is also true for the imaging of physical forces at work in living systems. Fluorescence imaging generally dominates as a method to elucidate biological processes in living systems, and elegant fluorescent probes have been devised for many purposes. However, the detection of physical forces in living systems is generally limited to strongly interfering physical tools or fluorescent probes integrated into larger bioengineered systems.^[1–16] What would be needed to enable much research in the life sciences are small-molecule fluorescent probes that can simply be added to living systems to report on physical forces. Around 2010, we thought we could tackle this challenge the way lobsters, crabs and shrimps change color during cooking (Figure 1).^[17–19] From this bioinspired concept of planarizable push-pull probes, fluorescent flippers emerged and are today available for use by the broader community. While scattered highlights on specific topics have appeared at different places for special occasions^[20–22] and a video for the lay public has been produced,^[23] a comprehensive account describing the creation of flipper probes in full is missing. With flipper probes approaching maturity, we thought the time is ripe for filling this gap.

2. The Emergence of Flipper Probes

The pigment that accounts for the color change of lobsters, crabs or shrimps during cooking is astaxanthin **1** (Figure 1).^[17–19] The orange color of cooked lobsters is that of astaxanthin itself, which is a carotenoid. Its chromophoric polyene is twisted out of conjugation because of steric

crowding from the methyl groups placed along the scaffold. This is true even in crystal structures. In living lobsters, astaxanthin is bound within a β -barrel, β -crustacyanin, which mechanically flattens the polyene. The result is an increase in conjugation along the polyene that translates into a red shift of absorption. The protein also polarizes the chromophore by hydrogen bonding to the ketone π -acceptor at one end and the tautomeric enediol π -donor at the other end of the polyene into a push-pull system that accounts for an additional red shift. Higher-order supramolecular effects further contribute to the final red shift. In other words, the spectacular color change we see in the kitchen is caused by nothing else than thermal protein denaturation, which liberates the pigment to relax in the twisted conformation with the orange color.

Similar combinations of planarization and polarization in the ground state account for the chemistry of vision, particularly color vision.^[24,25] However, the same concept has not been explored explicitly with fluorescent probes. Encouraged by early studies on the planarization of astaxanthin **1** by mechanical compression^[17] and twisted push-pull systems **2** in lipid bilayer membranes,^[26,27] we decided to launch the “lobster probe” project. The first planarizable push-pull probe **3** appeared in 2012.^[28] Oligothiophenes were selected as scaffolds because of expertise available from studies on artificial photosystems.^[29] The four thiophene rings are driven out of co-planarity by methyl groups along the scaffold, and terminal donor and acceptor build up the push-pull system. As expected, this probe reported the increasing order of surrounding lipid bilayer membranes by red shift of the excitation band. This proof-of-principle was not well received in the community because red shifts, that is the mechanosensitivity, and fluorescence were barely detectable. To improve on both, two thiophene rings in **3** were bridged with a pseudo-sulfide donor, while the other two were bridged with a pseudo-sulfone acceptor to give the flipper probe **4**.^[30] This structural modification aimed at increasing monomer fluorescence and surface area to better feel the environment, an operation that is reminiscent of putting on shiny flippers at a molecular level. The probe **4** was further equipped with push-pull donors and acceptors as well as a terminal carboxylate for amphiphilicity to ensure its delivery and orientation in lipid bilayers while minimizing background fluorescence as micelles in water. The finding of flipper probe **4** was not trivial, it took three years until **4** was published in 2015.^[30]

[*] Dr. X.-X. Chen, F. Bayard, N. Gonzalez-Sanchis, Dr. K. K. P. Pamungkas, Dr. N. Sakai, Prof. S. Matile
Department of Organic Chemistry, University of Geneva
1205 Geneva (Switzerland)
E-mail: stefan.matile@unige.ch
Homepage: <http://www.unige.ch/sciences/chiorg/matile/>

© 2023 The Authors. Angewandte Chemie International Edition published by Wiley-VCH GmbH. This is an open access article under the terms of the Creative Commons Attribution Non-Commercial License, which permits use, distribution and reproduction in any medium, provided the original work is properly cited and is not used for commercial purposes.

Flipper **4** excelled in model membranes with a highly mechanoresponsive excitation maximum and strong fluorescence. However, in cells, flipper **4** was toxic and distributed over all membranes without selectivity. These unfavorable properties were attributed to the elimination of the head group, which produces a reactive carbocation that can randomly react with weak nucleophiles (Figure 1, red arrow).^[31] The best solution for this problem was to attach the head group through a synthetically convenient triazole, while preserving the essential phenyl (i.e., thiophen-2-ylmethyl) oxygen for a large red shift (see below). In flipper **5**, protonation of phenyl ether leading to acid catalyzed head group elimination is hindered by charge repulsion^[32] from the neighboring weakly acidic protonated triazole.

Added to cells, flipper **5** labeled the plasma membrane selectively and showed excellent mechanosensitivity, negligible cytotoxicity and manageable phototoxicity under meaningful conditions. Two more years were necessary to fully characterize and understand the fluorescence response to membrane tension, before flipper **5** could be finally presented as a fluorescent membrane tension probe.^[33] Because of overwhelming demand from research groups worldwide, this original probe **5** was commercialized in 2018 and trademarked as Flipper-TR®. Since then, the emphasis shifted to different forms of intracellular targeting to enable use in biology as broadly as possible. Milestones in the design of the flipper mechanophore as such were the introduction of chalcogen-bonding cascade switches **6** in 2019^[34] and “blinking” dynamic covalent flippers **7** one year later for super-resolution microscopy^[35] and dual sensing of membrane compression and hydration.^[36] From **4** to **7**, structural changes were relatively minor, but had important consequences for function. Most attempts at major structural modifications resulted in failures, testifying to the complexity of the challenge and calling for much persistence to advance.

3. Synthesis

Flipper-TR® **5** is currently synthesized in 15 steps from commercially available starting materials (Scheme 1).^[20] The monomer unit, a dithieno[3,2-*b*:2',3'-*d*]thiophene (DTT), is prepared via double annelation reactions pioneered by Holmes and co-workers.^[37] In the first step, dianions



Stefan Matile is a Professor at the University of Geneva, Switzerland, and a founding member of the National Centre of Competence in Research (NCCR) Chemical Biology and the NCCR Molecular Systems Engineering. He received his education from University of Zurich (Ph.D.) and Columbia University, New York (postdoc), and started his independent career as an Assistant Professor at Georgetown University, Washington DC.

obtained from tetrabromothiophene **8** undergo addition reactions to acetaldehyde **9**. The resulting diol **10** is oxidized to diketone **11**. The following double cascade cyclization combines aromatic substitutions of dibromide **11** with thiols **12**, aldol cyclizations, and dehydrations to form the DTT core in **13**. Ester hydrolysis and decarboxylation of the resulting diacid **14** affords 3,5-dimethyl DTT **15** as the first key intermediate.

Aldehyde **16**, obtained by Vilsmeier–Haack formylation of **15**, is used in two directions. On the one hand, reduction with sodium borohydride and protection of the obtained alcohol **17** with a bulky solubilizing silyl group yields **18**. On the other hand, bromination of aldehyde **16** followed by a Schmidt reaction to convert aldehyde **19** into a cyano acceptor affords **20**. Oxidation of the pseudo-sulfide donor bridge in **20** into a pseudo-sulfone acceptor bridge occurs with MCPBA in high yield. Stille coupling of bromide **21** with the DTT **18** yields the dimer **22** in up to 73 % yield. From this key intermediate **22**, flipper **5** is obtained by first deprotection with TBAF followed by Williamson ether synthesis with bromide **24** and Cu^I catalyzed cycloaddition of the resulting alkyne **25** and azide **26**. Overall, flipper synthesis is feasible but not trivial, a nice example that substantial synthetic efforts are usually necessary to access significant function, and well justified if the function is truly significant.

4. Planarizable Push-Pull Probes

The original flipper probes such as Flipper-TR® **5** are DTT^[22,38–40] dimers twisted out of co-planarity due to methyl groups next to the single bond connecting the two monomers (Figure 2). The molecular electrostatic potential (MEP)^[41] surface of flipper **5** in planar conformation (**p**) shows that flipper deplanarization does not originate from steric hindrance but from electrostatic repulsion between the methyls and the σ holes^[42–49] on the endocyclic sulfur atoms (Figure 1). This repulsion represents the opposite of a chalcogen bond,^[42–49] that is “repulsive chalcogen bonding” or an “anti-chalcogen bond” (Figure 2). The mechanosensitivity of flipper probes is designed to originate from planarization by physical compression. The electrostatic origin of mechanophore twisting is therefore essential for function since twisting by steric repulsion is incompatible with planarization.^[50]

The primary push-pull system of flipper probes is composed of endocyclic donors (D_n) and endocyclic acceptors (A_n) bridging the two thiophenes in each monomer. Pseudo-sulfides as D_n and pseudo-sulfones as A_n have so far been the best and confirmed to be essential for function.^[51,52] This primary push-pull system is supported by exocyclic A_x and D_x . For A_x , nitriles, aldehydes and ketones have worked well. D_x was less straightforward to choose, because direct attachment of a conventional donor, such as an alkoxy group, to the already electron-rich DTT donor leads to its oxidative degradation due to the poor conjugation between donor and acceptor DTTs in twisted form.^[53] However, upon planarization, the presence of an exocyclic donor D_x is

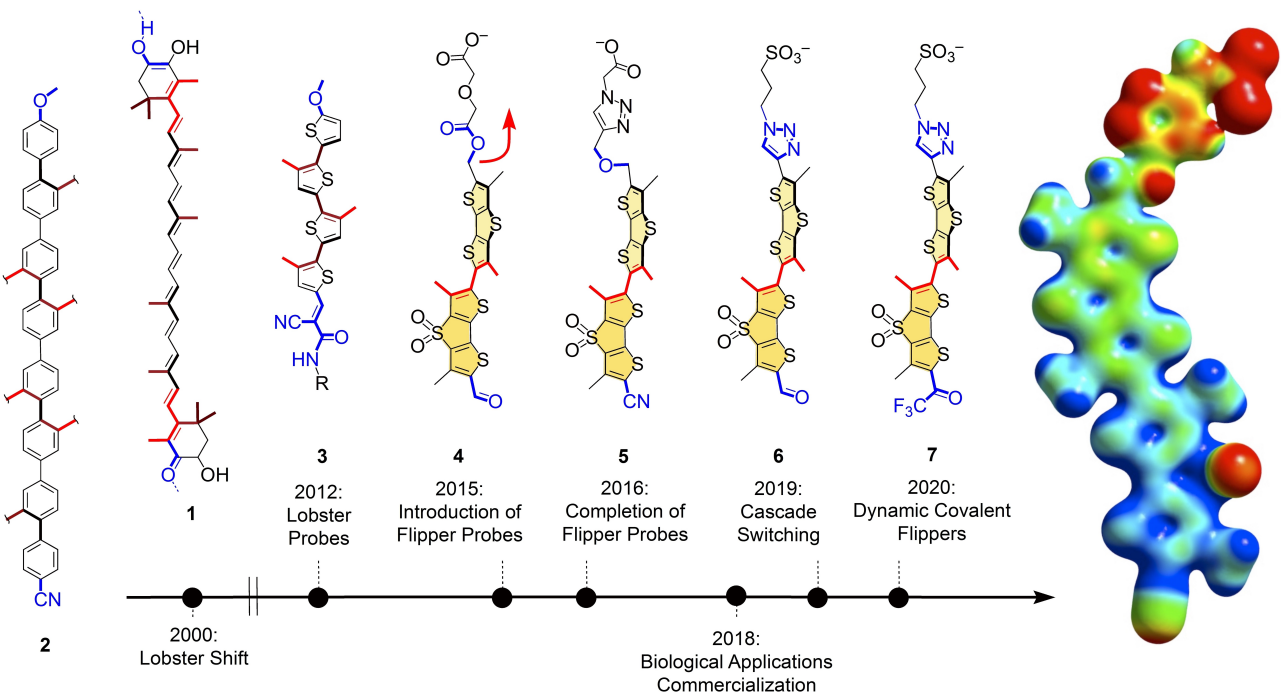
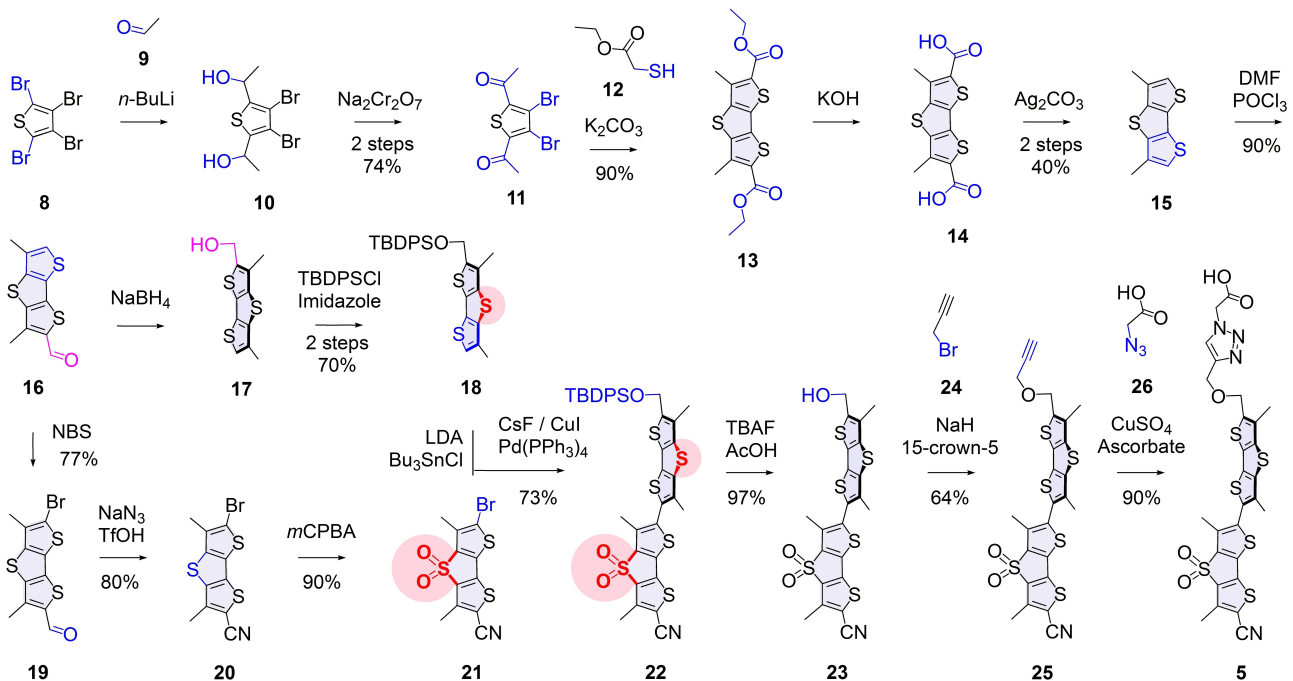


Figure 1. Timeline for the emergence of flipper probes, with MEP surface of Flipper-TR® 5 (red, electron rich; blue, electron poor). Counterions of anionic amphiphiles not shown. Adapted from Ref. [41].



Scheme 1. Synthesis of Flipper-TR® 5 in 15 steps from commercially available starting materials.

essential to generate a strong push-pull system that produces the red shifts and lifetime increases needed for mechanosensitivity. The solution for this dilemma is non-covalent chalcogen-bonding turn-on donors in general, for example, thienyl ethers in Flipper-TR® 5. In the twisted resting state **t**, the endocyclic sulfurs of electron-rich DTT donors have

shallow σ holes and are thus poor chalcogen-bond donors. The exocyclic non-covalent donors will thus not form chalcogen bonds and be turned off (Figure 2). In the planar conformation **p**, conjugation between the two DTTs is established to allow the transfer of electron density from the donor DTT to the acceptor DTT, resulting in the deepening

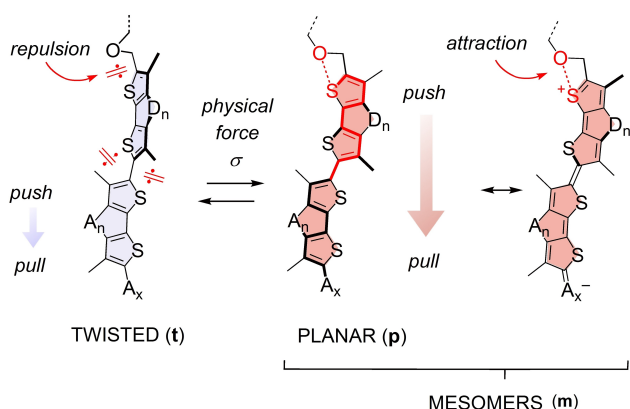


Figure 2. Mechanosensing with flipper probes by planarization and polarization in the ground state. General flipper structures are shown in twisted and planar conformation, with indication of general endocyclic (n) and exocyclic (x) acceptors (A) and donors (D), repulsive and attractive chalcogen bonding, push-pull dipoles and informative mesomers.

of σ holes on the sulfur atom at the donor end and the turning on of the chalcogen bond to inject electron density from the phenyl oxygen. The presence of chalcogen-bonding turn-on donors is essential for function, but its nature can change (see below).

The impact of flipper planarization is best illustrated with pertinent resonance forms. For example, one mesomer **m** shows the formation of a partial double bond between the monomers upon planarization that allows the flow of electrons from donor to acceptors, which results in a formal positive charge on sulfur to enable strong chalcogen bonds with the non-covalent turn-on donor. Other mesomers can be drawn to also illustrate how the other sulfurs and the methyl groups are participating as additional donors (bold, Figure 2).

4.1. Fluorescence Spectroscopy

In solution, flipper probes absorb at comparably short wavelength (Figure 3A, black, dashed), and the fluorescence is weak. Fluorescence quantum yields up to 30 % have been measured in EtOAc. Fluorescence is even weaker in water, obviating the need of washing steps in bioimaging. In liquid-disordered (L_d) lipid bilayer membranes, the absorption or excitation maximum red shifts to around 445 nm, and fluorescence intensity increases. In liquid-ordered (L_o) and solid-ordered (S_o) membranes, intensity further increases.^[30,31] The red shift of absorption and excitation maxima becomes most significant, and vibrational finestructure appears.^[35,54] Spectral deconvolution places the 0–0

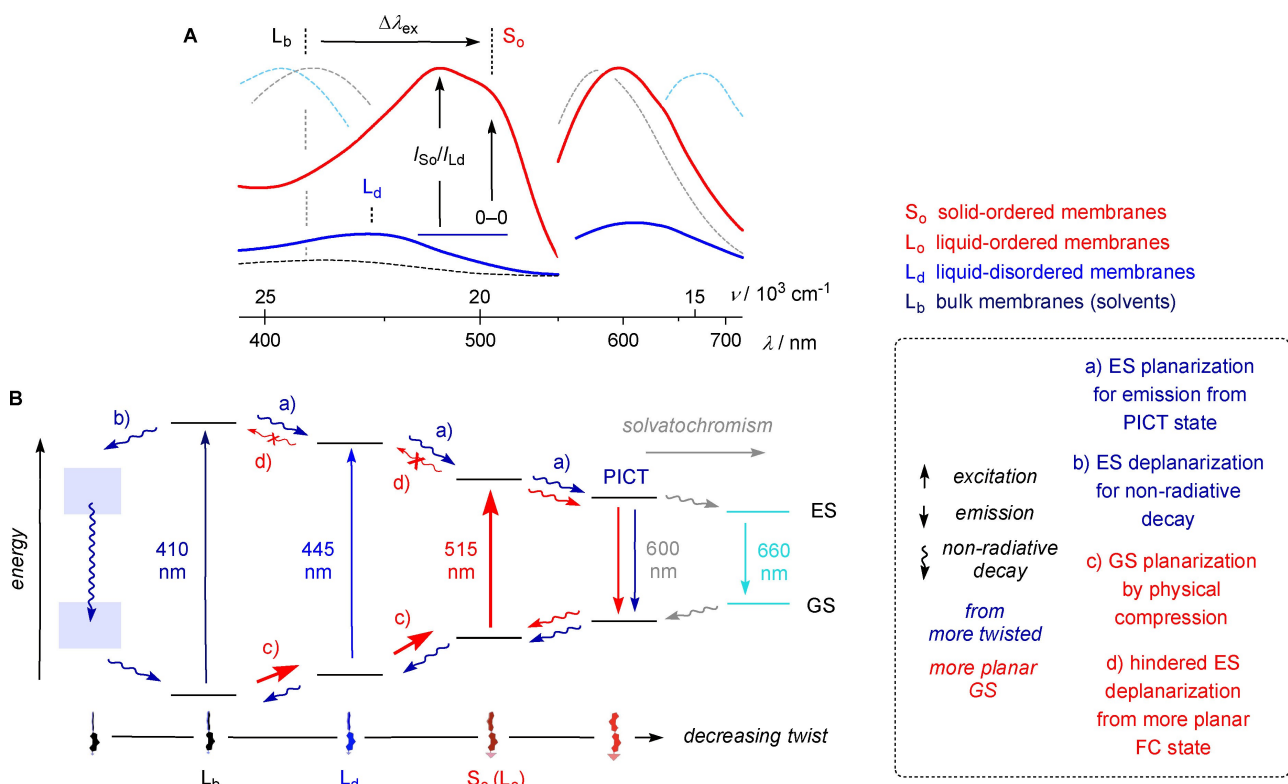


Figure 3. Excitation and emission spectra and energy diagram of flipper probes in liquid- (L_o), or solid-ordered (S_o , red), liquid-disordered (L_d , blue) and bulk membranes (L_b , black, grey, or cyan). A) Excitation and emission spectra of Flipper-TR® 5 in moderately (dioxane, dashed black and grey) without and with intensity normalization) and highly polar solvents (water, cyan; normalized), L_d (blue) and S_o membranes (red), with indication of red shift in excitation, intensity increase from L_d to S_o , and 0–0 transition in deconvoluted spectra. B) Energy diagram of flipper probes for ground state (GS) and excited state (ES) as a function of (c) mechanical planarization in the GS.

transition well above 500 nm, the 0–1 band slightly below. These red shifts of excitation/absorption maxima are consistent with flipper planarization in the ground state by physical compression in increasingly ordered membranes (Figure 3Bc). The extent of the red shift is important, around 100 nm from relaxed flippers in solution to highly planarized flippers in ordered membranes. Deconvolution of the vibrational finestructure appearing in more ordered membranes might inform on the perfection of positioning of flippers in the membrane leaflet, including the possible identification and quantification of smaller populations of mispositioned, dysfunctional flippers. Exhaustive control experiments exist to support that the original **5** and related flippers align along the lipid tails in one leaflet of the bilayer (depth quenching,^[30] computational simulations),^[55] do not affect the membrane structure significantly (Langmuir trough isotherms),^[56] act as monomers, partition almost equally between more and less ordered phases,^[30,52] show negligible flip-flop^[57] but transfer rapidly between different membranes.^[58]

The emission maxima do not shift significantly with membrane order (Figure 3A). In solution, the emission maxima of flippers show quite strong positive solvatochromism. Red-shifted emission was also found for planarized flippers on the water-exposed surface of G-quartets.^[59] In comparison, the solvatochromism in membranes is minor, thus revealing that the accessibility of water to membrane-bound flippers is as poor as expected from their alignment along the lipid tails of one leaflet.

The spectroscopic properties of flipper **5** add up to the energy diagram outlined in Figure 3B.^[20,21,59] Excitation from the twisted ground state in solution into the identically twisted Franck–Condon (FC) state is followed by ultrafast planarization (a)^[53] into a PICT (planar intramolecular charge transfer)^[60] state for emission into an equally planar ground state, which relaxes into the twisted steady state. This PICT state can be further stabilized by polar solvents, which causes the red-shifted emission known from positive solvatochromism. According to time-resolved emission spectroscopy, ultrafast planarization into the PICT excited state (a) occurs in a few picoseconds and is viscosity sensitive.^[53] Excited-state planarization is in competition with excited-state overtwisting for non-radiative decay through hypothetical TICT (twisted intramolecular charge transfer) states,^[60] conical intersections or other mechanisms (b),^[50,54] which reduces quantum yield and fluorescence lifetime of flipper probes.^[50,54]

Excitation of partially planarized flippers affords a partially planarized FC state at lower energy compared to the twisted FC state (Figure 3Bc). The resulting energy difference accounts for the red-shifted absorption and excitation maxima in response to flipper planarization in the ground state (Figure 3A). Independent of the degree of twisting in the ground state, emission always occurs from the PICT state, justifying why emission maxima do not shift much in response to ground-state planarization (Figure 3A). However, the competing overtwisting for non-radiative decay (b) is energetically unfavorable from less twisted FC states (Figure 3Bd). This hindered overtwisting accounts for

the increase of fluorescence intensity (Figure 3A) and lifetime in response to flipper planarization in the ground state.

4.2. Fluorescence Lifetime Imaging Microscopy

The responsiveness of flipper fluorescence lifetime to physical compression provides access to force imaging by FLIM (fluorescence lifetime imaging microscopy). This technique is attractive because fluorescence lifetimes are independent of concentrations, which are often difficult to determine and control in living systems. FLIM images of different flippers in GUVs (giant unilamellar vesicles) with L_d model membranes give lifetimes from 3.8 to 2.9 ns (Figure 4).^[30,54] In GUVs with L_o membranes, lifetimes from 6.4 to 5.5 ns are consistent with increasing flipper planarization in more ordered membranes. FLIM images of L_o GUVs further show increased anisotropy (dark equator regions), which is as expected with a tighter packing along the more ordered lipid tails.^[55] In GUVs with L_d and L_o domains, flippers like **4** and **5** label both (Figure 4, bottom). The L_o domain labeling is more intense. This is not because of preferred partitioning, which is compared to other probes remarkably good for L_o , almost as good as for L_d , depending on the nature of lipids and flipper.^[30,52] However, the labeling of L_o is more intense because of the higher oscillator strength of planarized flippers (Figure 3A), which produces more counts in the FLIM images. This apparent labeling of membranes with highest order is important to understand flipper properties in cells.

4.3. Imaging Membrane Tension in Living Cells

Membrane tension is the counteracting force against mechanical stretching of lipid bilayer membranes.^[1–16] FLIM imaging of GUVs and cells was used for the quantitative calibration of fluorescence lifetimes to membrane tension.^[33]

According to above energy diagram (Figure 3B), lifetime changes of flipper probes recorded in FLIM images report exclusively on the planarization of the twisted push-pull

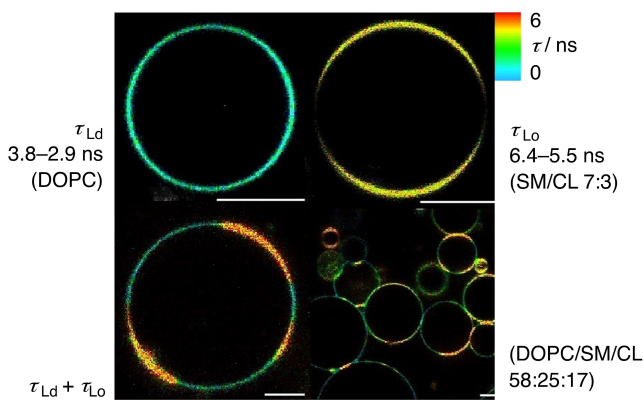


Figure 4. Representative FLIM images of flippers in GUVs with L_d , L_o and mixed membranes. Adapted from Ref. [54].

probe in equilibrium in the ground state. Responding to changes in membrane tension, FLIM images of flipper probes will report exclusively on changes in physical membrane compression (except for HydroFlipper 7, which simultaneously reports also on membrane hydration, see below). In all situations, solvatochromism is not involved in the imaging of membrane tension by FLIM.

Membrane tension was applied by micropipette aspiration or osmotic stress. Forces were determined from the diameter of nanotubes pulled from the GUV with optical tweezers. In homogeneous membranes composed of one type of lipid, fluorescence lifetimes decrease with increasing tension. This is consistent with lipid decompression dominating the response to the applied force (Figure 5A). This allows the partially planarized flippers in L_d or L_o membranes to relax into more twisted conformers, which

promote competing overtwisting in the ES for non-radiative decay, thereby shortening lifetimes (Figure 3Bb and Bd).

In cellular membranes and in heterogeneous model membranes composed of different lipids, lifetimes increase with growing tension. This demonstrates that the response to the applied force is dominated by membrane reorganization (Figure 5B). The sorting out of unstretchable lipids into highly ordered microdomains has been reported previously^[61–63] and could be reproduced with flipper probes by micropipette aspiration of GUVs composed of lipid mixtures near phase separation.^[33] Because of their high fluorescence intensity due to hindered overtwisting in the excited state (Figure 3Bd), the more planarized flippers in these out-sorted, highly ordered microdomains then dominate the total response and produce the observed increase in fluorescence lifetime (Figure 3Bc and Bd). According to flipper response, tension-induced dis/assembly of microdomains occurs generally in most cellular membranes. This observation suggests that the regulation of biological functions, such as signal transduction, by membrane tension is induced by changes in microenvironment of membrane proteins causing conformational changes that in/activate intracellular active sites. The dependence of fluorescence lifetime changes on the applied tension was quasi-linear up to at least 0.7 mNm^{-1} , with the slopes dependent on membrane composition.^[33]

In living cells, it is important to understand that the recorded lifetimes report on both membrane order, determined by their lipid composition, and membrane tension, determined by the applied force. These contributions can be dissected experimentally in the biological functional context. For instance, lifetimes recorded with flippers in plasma membranes exceed the lifetimes of flippers in the ER (endoplasmic reticulum, Figure 6A vs B).^[64,65] Differences in membrane order, rather than tension, account mostly for these different lifetimes recorded in plasma membranes and ER. The application of hyperosmotic stress to cells causes a

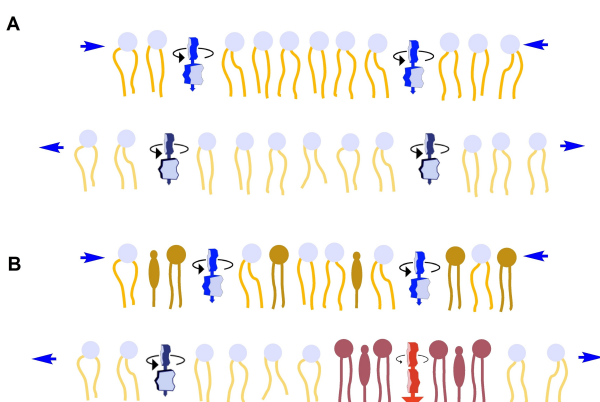


Figure 5. Response of flipper probes to physical forces applied to lipid bilayer membranes (blue arrows). A) In uniform membranes, lifetimes decrease with tension because lipid decompression dominates the response. B) In mixed membranes, lifetimes increase with tension because membrane reorganization, particularly tension-induced microdomain dis/assembly, dominates the response.

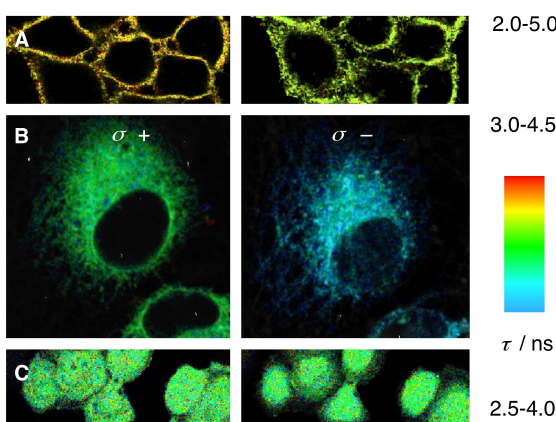


Figure 6. Protocol to image membrane tension in living cells. A)–C) FLIM image with flippers in plasma membrane (A) and ER (B) compared to rhodamine in the cytosol as negative control (C) without (left) and with hyperosmotic stress (right). D), E) FLIM histograms for B (D) and C (E), red, isotonic; black, hypertonic. F) Fluorescence lifetimes for cells in B, C and Golgi (GA); red, isotonic; black, hypertonic; from FLIM histograms (D, E), 1 diamond = 1 measurement, with solid black line corresponding to mean values, whiskers to standard deviation, solid grey lines to matching measurements on the same cell (**** $p < 0.0001$; ns, not significant). Adapted from Ref. [65].

decrease in fluorescence lifetime of flippers in plasma membrane and ER (Figure 6A, B). This difference in lifetime before and after osmotic shock originates from differences in membrane tension and their consequences in membrane organization. An illustrative example from biology are the long lifetimes found at the constriction site of dividing mitochondria, which originate from changes in membrane tension and their impact on membrane organization.^[64,66] This correlation of membrane tension with biological functions such as mitochondrial fission makes tension imaging in living systems so important and flipper probes so useful in the life sciences.

For quantitative analysis of lifetime changes in FLIM images of living systems, FLIM histograms are recorded. Different lifetimes from separate measurements are then averaged to yield the mean values with the experimental error. For example, the FLIM histogram for flippers in the ER confirms and quantifies the response to changes in membrane tension (Figure 6D) that is already visible looking at the FLIM image (Figure 6B).^[65] Rhodamine bound to a HaloTag in the cytosol without any contact to membranes is shown as an example for negative controls. Insensitivity to osmotic stress is already visible in the FLIM images (Figure 6C) and confirmed in the FLIM histogram (Figure 6E).^[65] A comparison of separate experiments shows that the reproducibility of absolute lifetimes is good but not perfect, which is reasonable because different cells are never fully identical (Figure 6F). Absolute flipper lifetimes should thus never be overestimated. However, the reproducibility of lifetime changes in response to changes in membrane tension is reliably high, each line in the plots in Figure 6F represents an individual experiment. This conclusion is generally valid. It holds for tension sensitive flippers in the ER compared to tension insensitive rhodamine in the cytosol, the latter showing one characteristic outlier. It is true also for flippers in the Golgi apparatus, which show overall higher absolute lifetimes compared to ER because of generally higher membrane order but similarly good reproducibility of these absolute values and excellent reproducibility of the same lifetime changes in response to membrane tension (Figure 6F).^[65] Technical know-how integrating lessons learned during 5 years of FLIM with flippers in living systems is currently becoming available.^[67]

5. The Flipper Collection

To enable tension imaging in intracellular organelles where physical tools would hardly reach, such as above mentioned ER, Golgi apparatus (Figure 6B, F) or mitochondria, a collection of flipper probes **27–34** has been built within five years since the introduction of Flipper-TR® **5** in 2018 (Figure 7). All members of the flipper collection operate with the same mechanophore introduced with the original Flipper-TR® **5**. Flipper targeting is achieved either with empirical tracker motifs for use in unmodified cells or with non-empirical cellular engineering methods.^[68–70]

Flipper-TR® **5** contains a terminal carboxylate for retention at the plasma membrane (Figures 6A and Fig-

ure 7). Other parameters contribute to the overall difficult selective labeling of the plasma membrane. Tracking of mitochondria, ER, and lysosomes with flippers **27–29** is more straightforward because the existing methods are very reliable.^[20,64,68–71] Mito Flipper-TR® **27** accumulates in mitochondria because their strong inside-negative membrane potential drives the permanent hydrophobic triphenylphosphonium cation across the inner membrane and prevents its release. The pentafluorophenyl group of ER Flipper-TR® **28** reacts with thiolates of proteins on the ER surface facing the cytosol. A long PEG-tether is inserted to ensure that covalently captured flippers still reach the outer leaflet of the ER membranes. The high acidity of the morpholino cation allows Lyso Flipper-TR® **29** to enter lysosomes and late endosomes by transient deprotonation to cross their membranes in neutral form, whereas the low pH inside these organelles prevents the same deprotonation for return into the cytosol (Figure 8). Like the original Flipper-TR® **5**, flippers **27–29** have been introduced early on and are already commercialized for use in the community.^[20]

5.1. Tracking Rules for Directional Penetration

The tracker series was recently enriched with EE-Flipper **33** and Arg-Flipper **34** (Figure 7).^[72,73] The objective was to assess the mechanics of early endocytosis. Universal tracking rules for unidirectional penetration along pH gradients were needed to tackle this challenge. As already mentioned, Lyso Flipper-TR® **29** is known to enter lysosomes by transient deprotonation to diffuse in neutral form across the hydrophobic membrane, while its return to the cytosol is not possible because low $pH \approx 5$ within lysosomes prevents transient deprotonation (Figure 8). Lyso Flipper-TR® **29** tracks also late endosomes, but fails to label early endosomes (EE) because their internal $pH > 6$ is too high to prevent transient deprotonation. The logical move was to decrease the acidity of the ammonium cation sufficiently so that transient deprotonation at $pH \approx 7.2$ in the cytosol is still possible but not at the slightly lower $pH > 6$ within early endosomes.^[32,74–76] Given the small difference in pH, it was not obvious that the approach would work. An increase of $pK_a = 7.4$ for the morpholino flipper **29** to $pK_a = 9.8$ for the dimethoxybenzylammonium flipper **35** resulted in about 40% EE tracking.^[72] This moderate labeling of early endosomes with internal pH 6.0–6.5 with a tracker of $pK_a = 9.8$ defines the dynamic range for transient deprotonation to $\Delta pK_a = 3.5$. It suggested that a pK_a just below $7.2 + 3.5 = 10.7$ would be ideal because this should still allow transient deprotonation in the cytosol to penetrate membranes in neutral form but hinder the return to the cytosol from the weakly acidic interior of EE. This is achieved with simple alkyl ammonium cations as in the side chain of lysine. EE-Flipper **33** with $pK_a = 10.6$ tracks about 70% of all early endosomes.^[73] EE-Flipper **33** labels also Golgi apparatus with internal pH 6.0–6.7. This could be interesting to perhaps label Golgi along the pH gradient from *cis* to *trans*. To eventually elucidate the mechanics of early endocytosis,

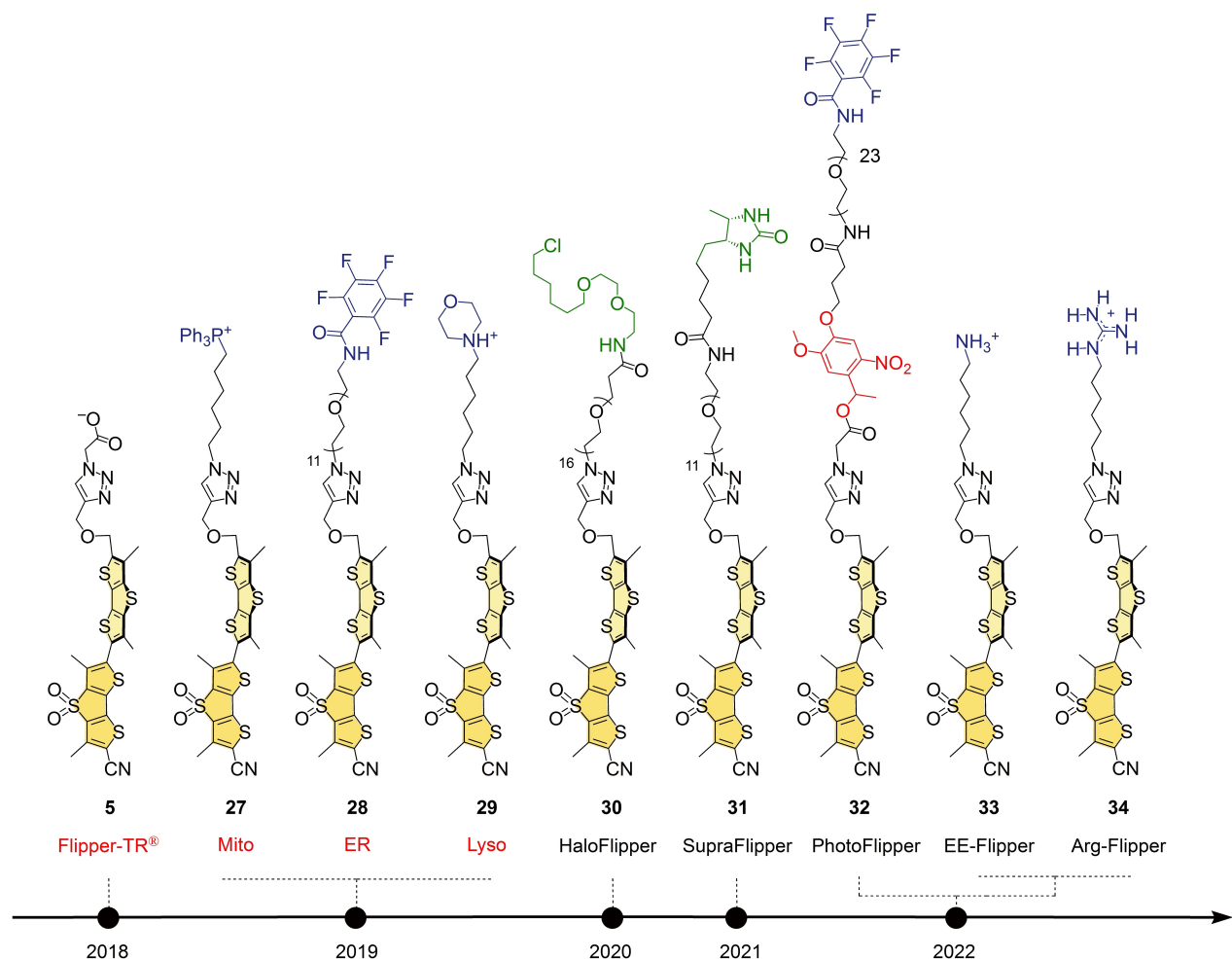


Figure 7. Timeline for the construction of the flipper collection for intracellular targeting. Red, commercially available.

signals from Golgi can be easily minimized by imaging above the nuclear plane.

Generality of the emerging tracking rules was probed with flipper **34** (Figure 7).^[73] The acidity of the guanidinium cation with $pK_a = 13.5$ as in the side chain of arginine^[77] is too weak for deprotonation in neutral water.^[78] Accordingly, Arg-Flipper **34** labels the plasma membrane. However, under different conditions, Arg-Flippers **34** self-assembles into “arginine-rich” micelles that penetrate cells efficiently and localize in mitochondria with high selectivity. Cell penetration of “oligoarginines” is as with cell-penetrating peptides and operates with repulsion-driven ion pairing rather than transient deprotonation.^[32] Attracted and trapped by the membrane potential like Mito Flipper-TR® **27**, cell-penetrating peptides have also been found accumulating in mitochondria.^[79] The same mechanism will thus apply to self-assembled or meanwhile disassembled Arg-Flippers **34**.

Plasma membrane labeling with monomeric Arg-Flipper **34** is special because the most intense fluorescence is observed in vesicles preparing for endocytosis and vesicles that are already ejected into the cytoplasm (Figure 8). With this unexpected ability of Arg-Flipper **34** to track the very

beginning, the flipper collection now provides full access to the mechanics of endocytosis. Excellent co-localization with EGF in CLSM images reveals that at least clathrin-mediated endocytosis is covered (Figure 8Bc). FLIM images of the same parts suggest that endocytosis starts with low tension and/or high disorder of membranes, in accordance with the literature. Although unlikely, contributions from labeled EGF call for cautious interpretation (Figure 8Bf).

5.2. HaloFlippers

Intracellular targeting by genetic engineering has the advantage that it is non-empirical and universal.^[68–70] The disadvantage is that the small-molecule membrane tension probes cannot be simply added to cells without prior engineering. This exactly is the advantage of trackers, which in turn have the disadvantage of being empirical and not universally applicable. HaloFlipper **30** was the first flipper developed for intracellular targeting by genetic engineering (Figure 7).^[65] The terminal chloroalkane reacts with an aspartate of an expressed HaloTag fusion protein in the membrane of interest (MOI). The resulting ester links the

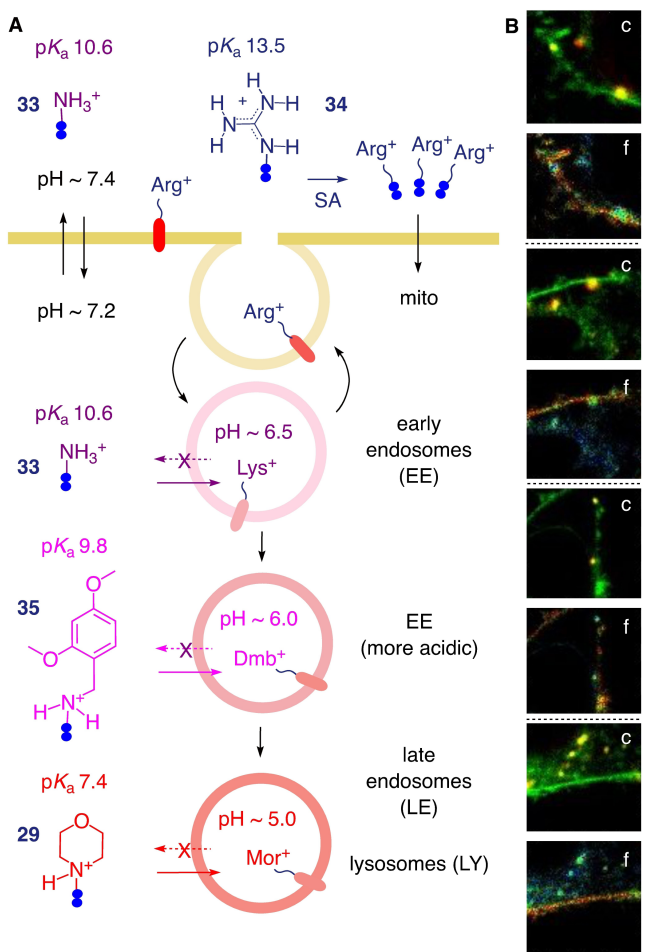


Figure 8. Flipper probes to elucidate the mechanics of endocytosis. A) Tracking rules developed for directional penetration along pH gradients provide access to lysosomes and late endosomes (29), early (35) and very early endosomes (33) by matching increasing pH with increasing pK_a . B) CLSM (c) and corresponding FLIM snapshots (f) with the permanent cation 34 highlight vesicle release from the plasma membrane. CLSM images show 34 (green) merged with internalized EGF (red), FLIM images long ($\tau = 5$ ns, red) to short lifetimes ($\tau = 3$ ns, blue) for 34. Adapted from Ref. [73].

flipper covalently to the HaloTag. The critical question in devising HaloFlipper 30 was to find the right tether length that enables the flipper to insert into the membrane but still penetrate cells efficiently. Although not fully generalizable, the ethylene glycol 16-mer in flipper 30 works overall best. The results used to describe imaging methods were obtained with HaloFlipper 30 in ER, Golgi and cytosol (Figure 6F).

5.3. SupraFlippers

SupraFlipper 31 was introduced next to combine targeting by genetic engineering and release by chemical stimulation (Figure 7).^[57] The approach exploits the superb RUSH method for flipper mechanoimaging.^[80] The terminal des thiobiotin enables the probe to first target streptavidin expressed at the site of interest within cells and second be

released upon addition of the better binding biotin. For validation, SupraFlipper 31 are loaded together with streptavidin into GUVs. Fully twisted in neutral water, flippers do not fluoresce significantly under these conditions (Figure 3A). These dark GUVs are first mixed with control GUVs loaded only with a water soluble fluorophore (Figure 9A). After the addition of biotin, the membranes of the dark GUVs start to fluoresce immediately, while the membranes of the control GUVs remain dark (Figure 9B and C). This result demonstrates the release of silent SupraFlipper 31 from streptavidin to light up the accessible membranes without crossing them, that is their inner leaflet. In engineered cells expressing streptavidin in the ER, this translates to ER labeled with low intensity and short lifetimes before addition of biotin (Figure 9D). Upon biotin addition, lifetimes in the ER increase first, reflecting flipper release from the targeting streptavidin into the surrounding inner ER membrane leaflets (Figure 9E). With time, Golgi appears brightly labeled at longer fluorescence lifetimes together with the plasma membranes at even much longer lifetime (Figure 9F). The evolution with time demonstrates that the chemically released SupraFlipper 31 move along the secretory pathway, available to explore changes in membrane order as well as the physical forces at work.

5.4. PhotoFlippers

PhotoFlippers 32 were introduced next to access release with light rather than chemical stimulation after targeting (Figure 7).^[58] In PhotoFlippers 32, a photocleavable *ortho*-nitrobenzyl ether^[81] is inserted between flipper and the targeting motif. This targeting motif is freely variable beyond the shown ER tracker. Chloroalkanes for HaloTagging, for instance, have been prepared as well. ER Photo-Flipper 32 was attractive to tackle a daunting challenge in the field, that is to image biomembrane asymmetry (Figure 10). Labeling of the outer leaflet of the plasma membrane is trivial, whereas labeling of the inner leaflet usually requires cumbersome microinjection in biological studies.^[82] ER-PhotoFlipper 32 was found to selectively label the inner leaflet of the plasma membrane with the original Flipper-TR® 5 (Figure 10). The ER-tracker attaches the PhotoFlipper covalently to the outer surface of the ER (Figure 10a). Irradiation liberates Flipper-TR® 5 (b). Capable of freely hopping between membranes (b) but not of flip-flopping across bilayer membranes (e), Flipper-TR® 5 labels all membrane leaflets accessible from the cytosol. However, the inner leaflet of the plasma membrane is most intensely labeled because membrane order is highest and emission from planarized flippers gives higher lifetime counts (Figure 4 and 10Ab).

To verify that the photocaged Flipper-TR® 5 only labels the inner leaflet of the plasma membrane (b), the original Flipper-TR® 5 was added from the outside (c) and then removed again from the outer leaflet with BSA (d). Not obvious in the FLIM images (Figure 10A) but quantitatively detectable in the FLIM histograms (Figure 10B), flipper addition to the outer leaflet increases the lifetime to

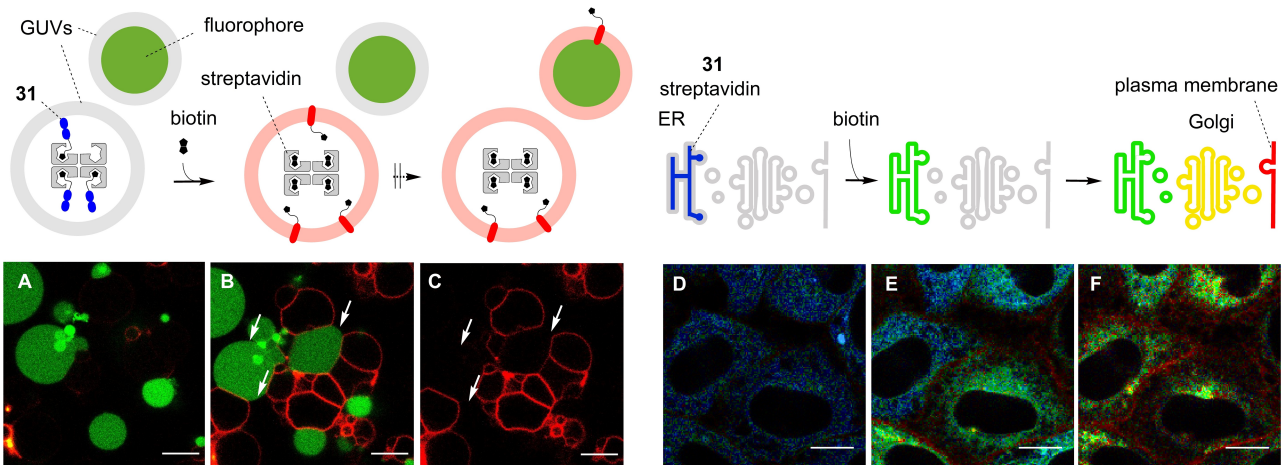


Figure 9. SupraFlippers 31 applied to access the secretory pathway. A)–C) CLSM images of SupraFlippers bound to streptavidin within vesicles mixed with fluorescent vesicles (A) before and (B, C) after the addition of biotin, confirming the absence of escape and vesicle hopping. D)–F) FLIM images of SupraFlippers bound to streptavidin expressed within the ER (D) before and (E, F) after the addition of biotin, confirming release into inner ER membrane leaflets followed by trafficking to Golgi and plasma membrane (blue short, red long lifetimes); scale bars 10 μ m. Adapted from Ref. [57].

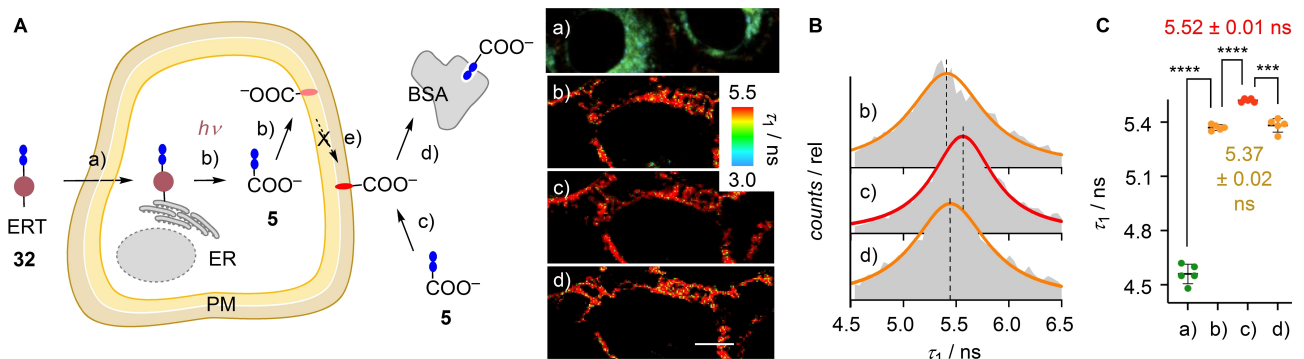


Figure 10. PhotoFlippers 32 applied to access plasma membrane asymmetry. A) Schematic representation of the processes and the corresponding FLIM images of HK cells after a) addition and b) irradiation of 32, c) addition of Flipper-TR® 5, followed by d) BSA; b) spontaneous membrane hopping, e) forbidden flip-flop; scale bar: 10 μ m. B) FLIM histograms for b–d. C) Fluorescence lifetimes for a–d; ***p < 0.0005, ****p < 0.0001. Adapted from Ref. [58].

5.52 ns, while subsequent removal lowers it back to 5.37 ns (Figure 10B and C). The lifetime in the outer leaflet calculated to 5.67 ns, that is 0.3 ns higher than in the inner leaflet. The conclusion that the inner leaflet of the plasma membrane is less ordered than the outer leaflet is consistent with the literature and biologically significant for membrane protein sorting, for instance.^[82] ER-PhotoFlipper 32 thus provides access to membrane tension imaging in both leaflets of the plasma membrane separately.

Another example of access to difficult membranes with Halo-PhotoFlippers concerns the labeling of the inner leaflet of the nuclear envelope upon photorelease from HaloTags expressed in the nucleus.^[58] The innermost leaflet of the nuclear envelope is hard to label because the nuclear envelope is an open bilamellar bilayer membrane with large pores and continuation into the ER.^[83] It is, however, important for tension imaging with regard to chromatin organization.^[84]

6. Chalcogen-Bonding Cascade Switches

The Achilles heel of current flipper probes are the exocyclic donors (Figure 1). The dilemma is that they are needed in planar flippers to obtain significant push-pull dipoles, red shifts and lifetimes, but undesired in twisted flippers to avoid oxidative decomposition (Figure 2). In Flipper-TR® 5, this dilemma is overcome with chalcogen-bonding turn-on donors (Figure 2), which give rise to perfect spectroscopic properties but fragilize the phenyl carbon. Elimination of the headgroup is further accelerated by acid-catalyzed activation of the leaving group (Figure 11, I),^[31] which can be sufficiently impeded in Flipper-TR® 5 by the presence of a proximal triazole proton scavenger (Figure 11, II).^[31] To tackle this problem, the fragile phenyl ether in Flipper-TR® 5 was replaced by a triazole directly attached to the DTT (Figure 11, III).^[34] At the same time, the acceptor was changed back from cyano group in 5 to an aldehyde as in

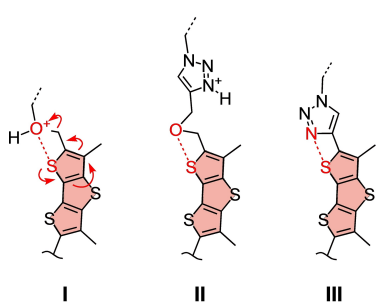


Figure 11. The dilemma with the exocyclic donor. Acid-catalyzed head-group elimination in **I** is suppressed by proximal triazole proton scavengers in **II** and avoided by deletion of the phenyl carbon in **III**.

6,^[34] or a trifluoromethyl ketone in **7** (Figures 1 and 12).^[35] The result is a chalcogen-bonding^[42–49] cascade switch (Figure 12). In the twisted form **7dt**, the two DTTs are decoupled. The sulfur near the triazole is thus electron rich, whereas the sulfur near the carbonyl is electron deficient. In this situation, the triazole nitrogen does not form the strong chalcogen bond needed to act as a non-covalent exocyclic donor, whereas the carbonyl oxygen can chalcogen bond and thus weaken its ability to serve as a covalent exocyclic acceptor in the twisted push-pull chromophore. The consequence is that both acceptor and donor are turned off in **7dt**.

Upon planarization, the two DTTs are in conjugation, electron density flows from donor to acceptor, which deepens σ holes on the donor and fills the σ holes on the acceptor side in **7dp** (Figures 2 and 12). The chalcogen bond to the triazole thus forms, and the one to the carbonyl breaks, which turns on both donor and acceptor. Operational chalcogen-bonding cascade switching was supported by

computational simulations, chemical stability of **7dt** and red-shifted absorption of **7dp**.^[34]

6.1. HydroFlippers

In HydroFlipper **7**, another level of complexity is imposed onto chalcogen-bonding cascade switches (Figure 1).^[35,36] Namely, a trifluoromethyl ketone^[85,86] is installed to reversibly turn off the exocyclic flipper acceptor in **7d** by dynamic covalent hydration (Figure 12A). Without strong push-pull system, the fluorescence of hydrate **7h** is weak, short-lived, and blue-shifted, in both twisted and planar conformation. The dynamic covalent exchange between bright **7d** and dark **7h** results in “blinking”, which is of interest for super-resolution imaging by single-molecule localization microscopy (SMLM). Characterized by PAINT-SMLM, HydroFlipper **7** resolves the thickness of a single bilayer of GUVs below diffraction limit.^[35] However, contributions from flipper hydration and flipper partitioning^[87] remain to be dissected, and for tension imaging, super-resolution FLIM would have to be introduced first.^[88]

Responding to dynamic covalent hydration and mechanical planarization, HydroFlipper **7d** should report on membrane hydration and membrane compression simultaneously. This dual imaging in a concentration and intensity independent manner could be realized by triexponential reconvolution of FLIM images.^[36] Separate peaks for the long-lived ketone **7d** and the short-lived hydrate **7h** appear in FLIM histograms (Figure 12B) together with one at very short lifetime for probably mispositioned flippers (not shown). The longer lifetime peak of the ketone **7d** responds to changes in membrane tension with shifts consistent with original flippers, reflecting mechanical probe compression

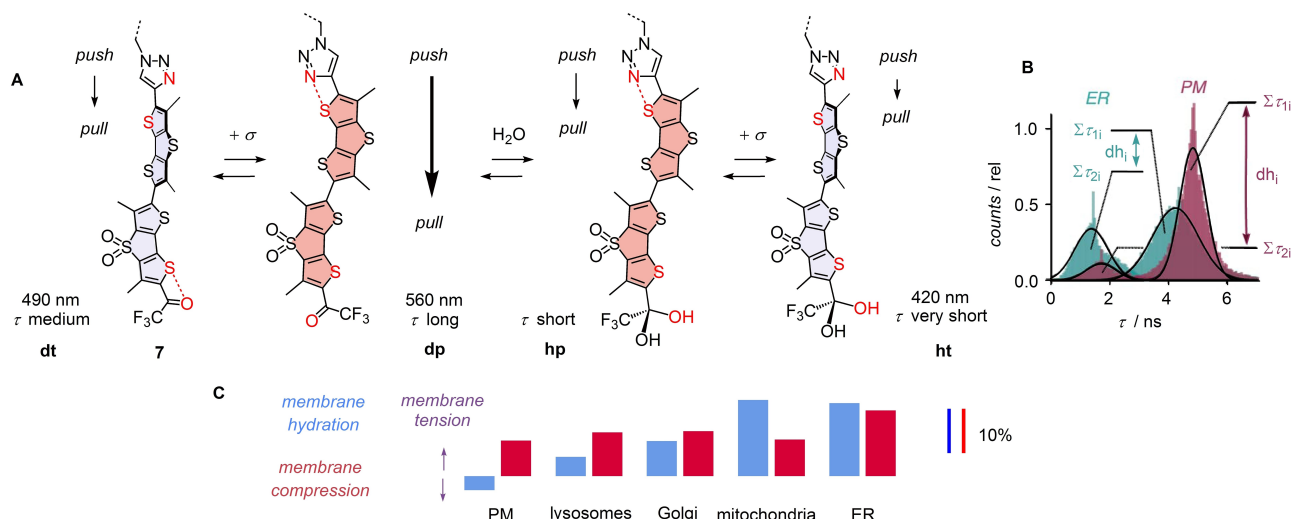


Figure 12. A) The dual sensing cycle of HydroFlippers **7**, combining twisted (t), planar (p), hydrated (h) and dehydrated (d) forms to simultaneously image membrane compression by planarization and membrane hydration by dynamic covalent ketone hydration. B) FLIM histogram from triexponential fit of fluorescence decay curves of pixels in FLIM images with the long lifetime 1 reporting on d (mechanosensitive) and the short lifetime 2 on h (mechanico-insensitive) of HydroFlippers in less hydrated plasma (purple) and more hydrated ER membranes (turquoise). The third population with very short lifetime is omitted. C) Trend plot for changes in membrane compression (red) and membrane hydration (blue) in response to changes in membrane tension. Adapted from Ref. [36].

(Figure 6D). For the short lifetime peak in the FLIM histogram, only negligible shifts are observed in response to membrane tension, which is consistent with absence of a strong push-pull system established upon planarization of the hydrated flipper **7h**.

Membrane hydration is of interest for bioimaging because it decreases with increasing membrane order. In the FLIM histogram of HydroFlipper **7**, the ratio of the counts for the long divided by the short lifetime peak was expected to report on membrane hydration. Indeed, this ratio is, for example, large in the more ordered plasma membrane (purple) and much smaller in the less ordered ER membranes (Figure 12B, green).

The dual sensing of membrane hydration and physical compression achieved by HydroFlipper **7** thus allows to compare their response to changes in membrane tension in the same experiment (Figure 12C). This was realized in different organelles tracked with HydroFlippers **7** as described above for Flipper-TR® **5** (Figure 7). The response of the planarizable push-pull probe **7** in the ground state to the lowering of membrane tension is a uniform decrease of lifetimes of the long lifetime peak in the FLIM histogram by >10%, independent of the nature of the membrane (Figure 12C, red). In contrast, changes in hydration of flipper **7d** give a scattered response to changes in membrane tension, from negative to strongly positive, dependent on the nature of the membrane, overall increasing with increasing intrinsic hydration of the membrane (Figure 12C, blue). These results indicate that membrane tension is reported more reliably by membrane compression than membrane hydration. This conclusion is important because it validates flipper design, that is the physical compression of planarizable push-pull probes in the ground state, as most appropriate to image membrane tension in living systems.

7. Reception

The comprehensive review of the use of flipper probes in biology is beyond the scope of this account focusing on flipper chemistry. To give a general impression, selected topics of flipper publications are summarized in Table 1.^[89–118]

The practical lessons learned during five years of cellular tension imaging with flipper probes are being communicated to facilitate use,^[67] and animations for the lay audience have appeared.^[23] “Ever heard of “fluorescent flippers”?” asks a tweet from independent users advertising a workshop taking place July 13, 2022 on the use of flippers to understand the morphogenesis in early mammalian embryo.^[119] Beyond scientific publications, this tweet illustrates how thanks to their availability, flipper probes spread in the community to enable research throughout the life sciences.

8. Alternative Probes

Extensive insights on flipper probes support that they report on membrane tension by responding to tension-induced

membrane reorganization (Figure 5B). This suggests that in principle, any fluorescent probe reporting on membrane order should be capable of imaging membrane tension. Many probes with these characteristics exist. The challenge is to find robust probes that report on membrane tension reliably and understandably. This is a challenge because probe response to tension-induced membrane reorganization depends on the extent the probe perturbs the surrounding membrane architectures (at best not at all, not like, e.g., cholesterol),^[56] probe positioning in differently ordered membranes (at best aligned to lipid tails, interference-free),^[30,56] partitioning between differently ordered domains in one membrane leaflet (at best without selectivity),^[30,52] flip-flop between the two membrane leaflets (at best absent),^[57,58] partitioning between membrane and medium, hopping between different membranes,^[58] concentration (beware of self-assembly), membrane composition, polarity, hydration, viscosity, potential, and so on. The reliability of probe response to these multiple parameters further depends primarily on how the probe transcribes the combined impact from membrane reorganization into a fluorescent signal (Figure 3B).^[36] The complexity of this challenge is alluded to throughout the manuscript, covering examples on the central importance to control and understand micro-domain partitioning (Figures 4 and 5) as well as flip-flop and hopping (Figures 8–10), and culminating in a quantitative assessment of signal transcription mechanisms that report reliably on membrane tension (physical compression) and others that do not (membrane hydration, Figure 12). All these insights are needed to identify the signature of robust probes. They are not predictable and require demanding experimental work.

Most of the current alternatives to flipper probes operate off-equilibrium in the excited state (Figure 13). The arguably best explored solvatochromic probes show red-shifted emission with decreasing membrane order (Figure 13Ad) because water, that is membrane hydration, stabilizes the ICT excited state (Figure 13Ac).^[120] Molecular rotors show increasing intensity and lifetimes with increasing membrane order (Figure 13Bc) because twisting in the excited state for non-radiative decay through formal TICT excited states or other mechanisms decelerates with increasing viscosity (Figure 13Bd).^[121–132] Although not studied so far in membranes, many probes for nucleic acid structures,^[133] or “aggregation-induced-emission”^[134] could operate in a similar manner. The origin of the mechanosensitivity of molecular rotors, responding to the kinetics of excited-state deplanarization (Figure 13Bd), is different from flipper probes, which mainly operate by ground-state planarization (Figure 3Bc). In contrast to rotors, the fluorescence of flippers weakens slightly with increasing viscosity,^[34] probably because of their viscosity-dependent ultrafast excited-state planarization (Figure 3Ba).^[53]

Probes that deplanarize by bending rather than twisting, referred to as flappers,^[135–138] papillons^[139,140] and the like, report on membrane organization by changes of the ratio of dual emission (Figure 13Cc, Ce), that is the viscosity-dependent kinetics of excited-state planarization (Figure 13Cd). Flipper-like ground-state planarization in equili-

Table 1: Biological applications of flipper probes.

Flipper probe	MOI	Studied correlation to membrane tension	Ref.
Flipper-TR® 5	Hepatic stellate cells	Matrix stiffness	[89]
"	Madin-Darby canine kidney (MDCK) cells	Cell volume changes	[90]
"	Human embryonic kidney (HEK293A) cells	YAP/TAZ, co-activators of the hippo pathway	[91]
"	Human umbilical venous endothelial cells	Flow (shear stress) and clustering of ICAM-1	[92]
"	Human lung cancer (Calu-1) cells	Hippocalcin-like protein 1 and cadherin 2 during ferroptosis	[93]
"	Breast cancer (MDA-MB-231) cells	PD-L1-mediated cell migration	[94]
"	Human aortic endothelial (tHAECS) cells	Shear stress and dependence on spectrin	[95]
"	Mouse embryo	ASPP2-dependent F-actin organization under mechanical stress at apical junctions	[96]
"	MDA-MB-231	Extracellular viscosity and migration of breast cancer cells	[97]
"	GUvs	Inflammatory lipid hydrolase cPLA ₂ , a nuclear membrane mechanosensor, and osmotic swelling in GUvs	[98]
"	Human bone osteosarcoma (U2OS) cells	Membrane reorganization during cellular uptake	[99]
	Human macrophage	The effect of 5-methyltryptophane, a macrophage differentiation factor, on mitochondrial membranes	[100]
Mito-Flipper-TR® 27	African green monkey kidney (Cos-7) cells	Mitochondrial membrane tension and fission	[66]
Flipper-TR® 5	Duchenne muscular dystrophy cardiac myocytes (DMD CM)	Restoration of membrane tension by truncated dystrophin proteins	[101]
"	MDCK	Epithelial folding in tissue morphogenesis, by applying out-of-plane deformations	[102]
"	Immortal human hepatic cell line (Huh-7)	The mammalian autophagy factor ATG9 A protecting against plasma membrane damage	[103]
Lyso Flipper-TR® 29	Human Pancreatic Ductal Carcinoma (KP4)	Myoferlin protecting lysosomal membranes against stress	[104]
Flipper-TR® 5	Human cervical cancer (HeLa Kyoto) cells	Thiol-mediated cellular uptake of cell-penetrating peptides	[105]
"	"	Cell volume changes during osmotic variations	[106]
Lyso Flipper-TR® 29	HeLa MZ	ESCRT-II-dependent intra-luminal vesicle formation during endocytosis	[107]
Flipper-TR® 5	HeLa	Membrane morphology manipulations using a new soft-gel nanoimprint lithography method	[108]
"	Mesenchymal stem cells	The impact of 3D gel matrix variation	[109]
"	Skin epidermis stem/progenitor cells	The response of the nuclear envelope to mechanical stretching of the cell	[110]
"	Insulin-secreting rat insulinoma (INS-1E) cells	Effects of the exposure to fatty acids	[111]
"	Breast cancer (HCC1937) and glioblastoma (T98G) cells	Effects of added synthetic lipids	[112]
"	GUvs	Functions of ether and sphingolipids in the secretory pathway	[113]
"	Human ovarian cancer (A2780) cells	Migration of epithelial cells, focusing on low tension in the rear when moving in a 3D-matrix	[114]
"	Yeast cells	Endocytosis, inhibition of target of rapamycin complex 2 (TORC2)	[115]
"	"	The inactivation of TORC2 with phosphatidylinositol-4,5-bisphosphate	[116]
"	Primary visceral adipocytes	The effect of high-fat-diet feeding on adipose tissue	[117]
"	HEK293T	Membrane reorganization by interferon-induced transmembrane (IFITM) proteins to inhibit viral entry	[118]

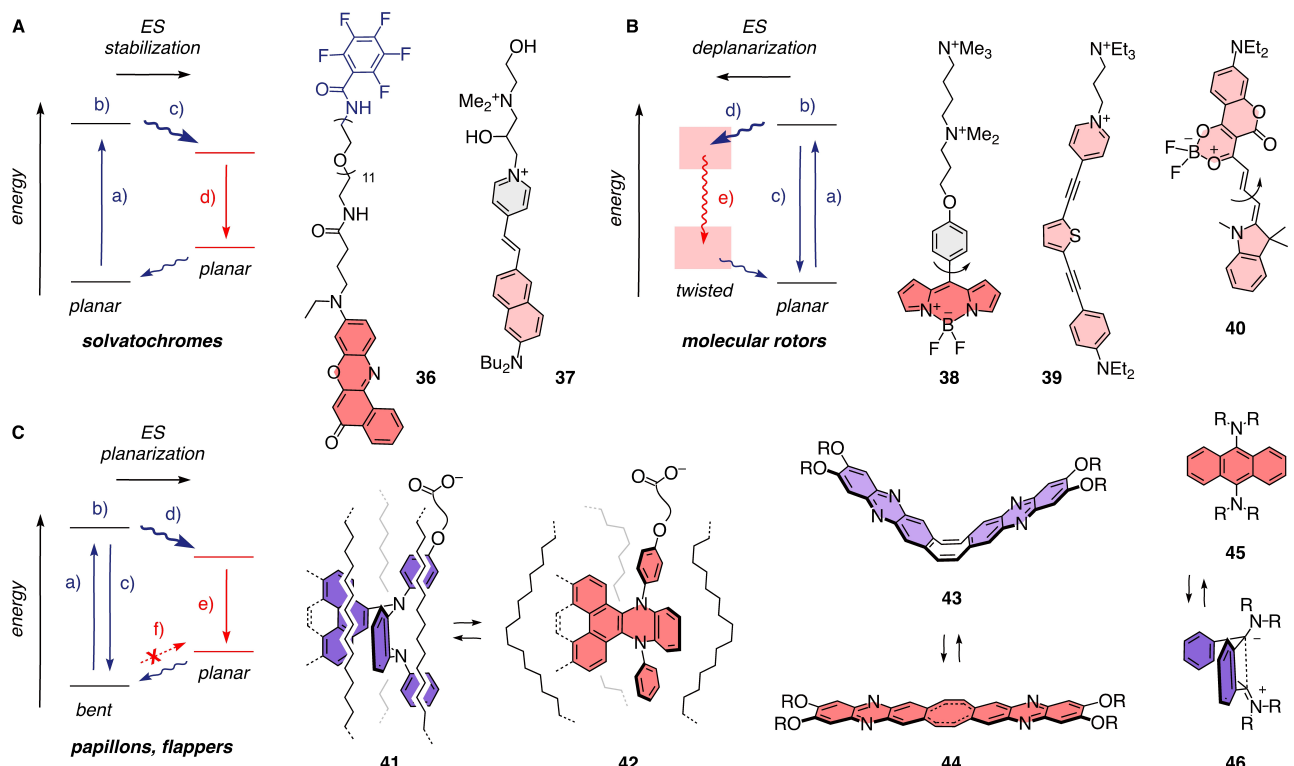


Figure 13. Possible alternatives to flipper probes operate off equilibrium in the excited state as either (A) solvatochromic probes, reporting on the stabilization of the excited state by polar solvents (c) (36–37), B) molecular rotors, reporting on the mechanosensitivity of twisting in the excited state (d) (38–40), and C) flappers, or papillons reporting on the mechanosensitivity of un/bending in the excited state (d) rather than in the ground state (f) (41–46).

brium by physical compression was conceivable also for the bent counterparts but so far not observed, presumably because energy demands are too high (Figure 13Cf).^[135, 139, 140]

Innumerable solvatochromic probes exist as potential candidates to image membrane tension in living systems.^[120, 141–143] Their assessment is most advanced with Nile Red probes, known for high sensitivity toward membrane order.^[120, 144] Klymenko and co-workers attached a variety of trackers to their Nile Red probe, including the standard ER tracker in **36** (Figure 13A).^[145] The response of the resulting probes to changes in membrane tension in ratiometric CLSM images varies strongly depending on the MOI. This strong and complex dependence on the nature of the different MOIs is as for membrane hydration imaged simultaneously with dual-sensing HydroFlipper **7** (Figure 12C, blue).

Di-4-ANEPPDHQ **37** ranks among the most established probes to image membrane order.^[82, 146, 147] In cells, Di-4-ANEPPDHQ stains the outer leaflet of the plasma membrane before being internalized. The inner leaflet labeling of the plasma membrane has been recently achieved by physical microinjection of this dye, nicely illustrating the need for less invasive chemical methods introduced with photochemical uncaging with PhotoFlipper **31** (Figure 10).^[82] Ratiometric imaging of plasma membrane tension has also been attempted using Di-4-ANEPPDHQ **37**.^[148]

The best explored molecular rotor in bioimaging is BODIPY **38** from Kuimova and co-workers. Chloroalkane versions as in HaloFlippers **30** have been targeted throughout cells to image microviscosity also in response to osmotic stress, without explicit discussion of the possible location of the probe.^[123] In an outstanding study, diyne **39** has been used by the same group as planar push-pull rotor to image non-classical responses of model GUV membranes to membrane tension.^[149] Very recently, **40** was introduced as planar push-pull rotor that might image membrane tension in model GUV membranes with unusually large changes of lifetimes, and target the ER.^[132]

Referred to as flappers^[135] or papillons,^[139, 140] mechano-phores that deplanarize by bending rather than twisting are attractive candidates for imaging membrane tension. Constant excitation maxima in model membranes reveal that high membrane order fails to planarize dihydronaphthalene-*a,c*-phenazines papillons **41** in the ground state, presumably because of the too high energy costs (Figure 13Cf).^[140] This difference underlines their distinct mode of action from flipper probes (Figure 3Bc), and supports the importance of flipper twisting by repulsive chalcogen bonds (Figure 2) to access torsional energies that match the tension range at work in mechanobiology. In the excited state, closed papillons **41** remain closed in ordered but open up into papillons **42** in disordered membranes.^[140] The resulting ratios in dual emission from bent and planar excited states

report on membrane order (Figure 13Cc, Ce). Despite reservations from weak fluorescence and blue-shifted absorption, papillons similar to **41** have been successfully used for imaging microviscosity without interference from polarity in living cells.^[150] Cyclooctatetraene-centered flappers like **43** similarly unbend in the excited state into planar **44** with increased conjugation for red-shifted emission.^[135]

While they work as mechanosensors in polymers and gels,^[135] studies in lipid bilayers have so far been unsuccessful (unpublished). Reporting off equilibrium on excited-state planarization, the bent flappers or papillons are thus more similar to excited-state deplanarization of twisted rotors than to ground-state planarization of flippers. Intriguingly, the reverse excited-state deplanarization of flappers **45** has been realized as well, due to the formation of the non-canonical Dewar-like benzene in **46**.^[151] Applications to bioimaging are of interest because non-radiative decay occurs through conical intersections rather than the multi-responsive hypothetical TICT states, but are so far still in their infancies.^[152]

The porphyrin dimers **47** and **48** with a dialkyne twister is unique for several reasons (Figure 14).^[122,153] Twisting occurs not because of steric or electrostatic repulsion, but because of the two alternatives available to conjugate with the two π bonds of the triple bonds. In GS and ES, planar and twisted porphyrin dimers **47** and **48** co-exist. The planar conformer **48** (Figure 14e-h) absorbs and emits red-shifted compared to the twisted **47** (a-d). The twisted **47** shows excitation and emission spectra of monomeric porphyrins, characterized by the Soret band (a), the Q band (b, d), and internal conversion (IC, c). Upon selective excitation of the twisted conformer **47** (a) followed by IC (c), viscosity-dependent planarization in the excited state can be observed (i), either from changing ratios of Q band emission (d/h) or from changing lifetimes for the twisted emission (d). Porphyrin dimers **47** and **48** have been studied in GUVs and cells, without special emphasis on planarization in the GS (j) as for flipper probes (Figure 3Bc). Related porphyrin dimers with only one alkyne twister have been explored early on to image membrane tension in polymersomes.^[154]

Dialkyne **49** has been introduced to form mechanosensitive ion channels that open up with increasing membrane

tension (Figure 14).^[155,156] This activation has been attributed to disassembly of transmembrane aggregates in response to mechanical lipid decompression. This disassembly was supported by a small blue shift of the emission maximum, which was assigned to a slow transition from excimer to monomer emission, without consideration of possibly increasing deplanarization.

Other approaches to image membrane tension include dynamic-covalent polymerization of amino aldehydes **50** into polyimines **51** (Figure 14).^[157] Increasing polymerization with membrane order due to membrane dehydration and, possibly, higher effective concentrations has been confirmed. However, this conceptually distinct mechanism of sensing membrane order in equilibrium in the ground state is of limited use because, contrary to expectations from the literature, only monomers **50** but not dynamers **51** do fluoresce.^[157]

Another representative example beyond small molecule probes concerns FRET-labeled DNA duplexes attached to cholesterol.^[158] These zipper probes report on membrane reorganization by duplex dis/assembly and the respective changes in FRET. Fluorescent probes have also been developed to report on membrane hydration by ES intramolecular proton transfer (ESIPT).^[159,160] An impressive series of fluorescent membrane probes that operate with photoinduced electron transfer (PeT) has so far been mostly explored to image membrane potentials.^[161]

Within the flipper family, many possible modifications have been tried without success. This collection of failed flippers includes monomers and anion-transporting trimers,^[162] removal of the primary dipole^[51] and variation of the primary, endocyclic acceptor (sulfoximines,^[52] preliminary phospholes,^[22,163,164] unpublished), variation of the exocyclic donors and acceptors, with particular efforts devoted to identify and overcome the dilemma of the exocyclic donor (see above).^[21,31,34,53,165] Key spectroscopic properties are weakened or lost upon deletion of the central methyls, affording planar push-pull rotors, or upon extension to ethyls, not to speak of larger groups.^[54] With central ethyls, performance is poor not because they hinder planarization but because they hinder flipper positioning along the lipid tails. The conclusion that literally every atom

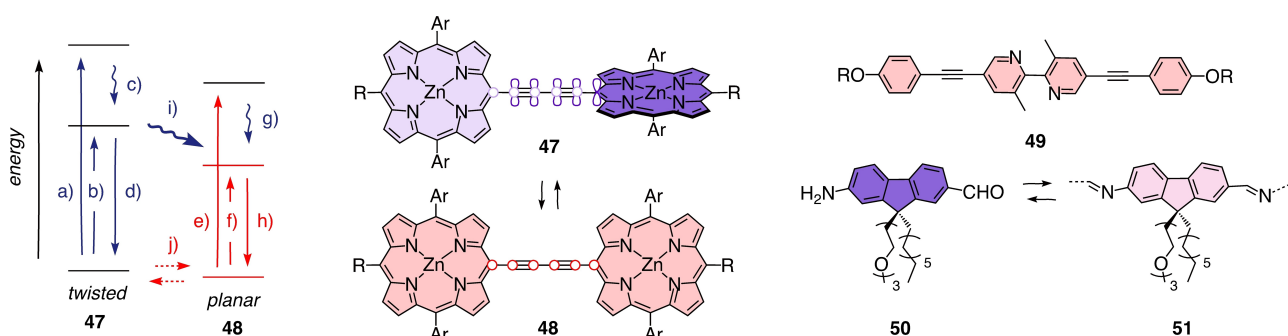


Figure 14. Upon selective irradiation of the twisted conformer (a) followed by internal conversion (c), porphyrin dimers **47**–**48** report off equilibrium on the mechanosensitivity of untwisting in the excited state (i). Mechanosensitive synthetic ion channels **49** report on the disassembly of excimers, and dynamers **51** on depolymerization in the ground state in equilibrium.

matters in flipper probes is overall meaningful and almost correct. Identified exceptions are the removal of the peripheral methyls next to the exocyclic donors and acceptors, which is allowed also in cascade switches without drastic consequences to the better or the worse.^[166] None of planarizable push-pull probes other than DTT dimers considered so far are functional in lipid bilayer membranes, including, for instance, twisted diketopyrrolopyrroles, i.e., Ferrari Red (unpublished).^[167]

Taken together, innumerable possibilities to image membrane tension with small molecules exist in theory, and preliminary tests have been reported for several candidates. One objective to write this account was to summarize lessons learned not only on how to design but also on how to evaluate and use small-molecule membrane tension probes meaningfully. For example, HydroFlipper 7 shows that probes responding to membrane hydration are not likely to report reliably on changes in membrane tension throughout cellular MOIs (Figure 12C, blue), while probes responding to physical compression are more likely to report reliably (Figure 12C, red).^[36] HydroFlippers 7 are excellent examples because they also illustrate the level of sophistication in probe design (Figure 12A), synthesis and evaluation (Figure 12B) that is required to secure the quantitative data, recorded simultaneously with the same probe, that allow to draw these conclusions with meaningful confidence.

9. Concluding Remarks

The fluorescence imaging of physical forces in biological systems with small-molecule probes is an important challenge in current life sciences. To contribute solutions, fluorescent flippers have been introduced as general probes to image membrane tension in cells. The general objective of this account was to summarize the emergence of fluorescent flipper probes for the broader community. We recapitulate how the bioinspired concept of planarizable push-pull probes has been introduced to achieve mechanosensitivity that reports on physical compression in equilibrium in the ground state, a novel mode of action that is distinct from other membrane probes that report off equilibrium in the excited state. The name “fluorescent flippers” further highlights the identified importance of strong monomer fluorescence and large surface area to achieve sufficient mechanosensitivity in membranes of different order. The resulting probes report increasing compression with red shifts in absorption rather than emission, as well as higher fluorescence intensity, quantum yield and lifetime. Increasing membrane tension in biomembranes is recorded as increasing lifetime in FLIM images because membrane reorganization, particularly tension-induced phase separation, dominates the response. Quantitative correlation of lifetimes with applied forces yields quasi-linear dependence up to 0.7 mN m^{-1} . Strategies to target any cellular membrane of interest with leaflet precision have been put in place using empirical tracker and non-empirical cellular engineering approaches, in combination with release by chemical stimulation or light. Examples

illustrate access to selective imaging of the mechanics along secretory pathway and endocytosis, inner and outer leaflet of plasma membranes, different endosomes, lysosomes, mitochondria, also during fission, Golgi, ER, nuclear envelope, with spatio-temporal control. Advanced flipper designs focus on the exocyclic donor, the Achilles heel of fluorescent flippers, blinking flippers for super-resolution imaging, and on dual sensing. The latter reveals that the responsiveness of flippers to physical compression reliably reports changes in tension throughout cellular membranes of interest, while the responsiveness to tension-induced changes in membrane hydration is more random.

The design and the evaluation of small-molecule tension probes turns out to be much more challenging than they might appear. The difficulty is not to find probes that image membrane order, there are many. But too many interconnected parameters influence the fluorescence response to membrane reorganization caused by tension. Because of these interconnected parameters, the sensitivity of the operational probe toward structural changes is exceptionally high and far from predictable, literally every atom counts, as a long list of failed flippers and alternatives testifies.

Taken together, fluorescent flippers emerge as a fine example of translational supramolecular chemistry, where the integration of fundamental, often novel supramolecular principles ends up satisfying a central need in the larger community. Flipper probes thus support the general expectation from translational supramolecular chemistry that offering different, underrecognized, at best new ways to get into contact on the molecular level will provide access to new structures and functions that could allow us to ultimately crack otherwise intractable challenges in science and society.

With operational membrane tension probes in place, the most important perspectives with fluorescent flippers relate to their use in the life sciences. Preservation and expansion of flipper distribution thus deserves high priority, particularly with regard to also making the most practical probes such as HaloFlippers available for the community. Lessons learned with flipper probes will help to find other, perhaps better probes. Fluorescent flippers themselves, although operational, are far from perfect. With membrane reorganization dominating the response to tension, control over interdomain partitioning (Figure 5B), intermembrane transfer (Figures 9 and 10), flip-flop (Figures 9 and 10) and sensitivity toward membrane thickness, subphases, potential^[161,29] and so on, without losses in performance, deserves highest attention and is exceptionally difficult, as alluded to throughout the text. While cytotoxicity is unproblematic, phototoxicity is intrinsic and manageable^[67] but appears improvable, particularly with regard to blebbing upon prolonged irradiation. Chemical stability is acceptable but far from perfect (Figure 11), breaking the six-nano-seconds barrier for fluorescence lifetimes is one of the next milestones (Figure 4), and super-resolution imaging (Figure 12) of membrane tension over time is yet to come.

To close, on a more anecdotal note: The largest red shifts of flipper probes have been observed in frozen DMSO-*d*₆ (Figure 15). Upon freezing a solution of flippers



Figure 15. Freeze-thaw cycle of flipper probes in $\text{DMSO-}d_6$ in liquid nitrogen and hot water (top, left to right), compared to cooked and raw shrimps (bottom).

in an NMR tube, its orange color turns brownish-black, while melting in warm water restores the original orange color (Figure 15, top, left to right). This color change is exactly the color change of lobsters, crabs, or shrimps during cooking (Figure 15, bottom), with the only difference being that it can be repeated many times. Considering that flipper design was originally inspired by the release of planarized and polarized astaxanthin **1** into its relaxed twisted ground state by thermal protein denaturation during cooking (Figure 1), the matching color changes found in freeze-thaw cycles in $\text{DMSO-}d_6$ felt like mission accomplished. The observation is obviously irrelevant for the imaging of membrane tension in living systems, and fine black powder spotted during the melting process also supported that such extraordinary shifts of biological and synthetic planarizable push-pull probes require additional contributions from more complex higher-order supramolecular chemistry. Because of its lacking significance for tension imaging, the molecular basis of the “black flipper” is unknown until today.

Acknowledgements

We are grateful to the many past and present co-workers and collaborators who contributed to the emergence of fluorescent flipper probes, thank M. Riggi for the frontispiece, and the University of Geneva, the National Centre of Competence in Research (NCCR) Chemical Biology (51NF40-18598), the NCCR Molecular Systems Engineering (51NF40-182895), and the Swiss NSF for financial support (Excellence Grant 200020 204175, Swiss-ERC Advanced Grant TMAG-2_209190). Open Access funding provided by Université de Genève.

Conflict of Interest

The University of Geneva has licensed Flipper-TR® probes to Spirochrome for commercialization.

Data Availability Statement

Data sharing is not applicable to this article as no new data were created or analyzed in this study.

Keywords: Bioimaging · Fluorescent Probes · Mechanochemistry · Membrane Order · Membrane Tension

- [1] B. Pontes, P. Monzo, N. C. Gauthier, *Semin. Cell Dev. Biol.* **2017**, *71*, 30–41.
- [2] R. J. Leiphart, D. Chen, A. P. Peredo, A. E. Loneker, P. A. Janmey, *Langmuir* **2019**, *35*, 7509–7519.
- [3] Y. Liu, K. Galior, V. P.-Y. Ma, K. Salaita, *Acc. Chem. Res.* **2017**, *50*, 2915–2924.
- [4] P. Keshri, B. Zhao, T. Xie, Y. Bagheri, J. Chambers, Y. Sun, M. You, *Angew. Chem. Int. Ed.* **2021**, *60*, 15548–15555; *Angew. Chem.* **2021**, *133*, 15676–15683.
- [5] A. Saric, S. A. Freeman, *Front. Cell Dev. Biol.* **2021**, *8*, 611326.
- [6] E. J. Aird, K. J. Tompkins, M. P. Ramirez, W. R. Gordon, *ACS Sens.* **2020**, *5*, 34–39.
- [7] Q. Feng, B. Kornmann, *J. Cell Sci.* **2018**, *131*, jcs218479.
- [8] M. C. Piontek, R. B. Lira, W. H. Roos, *Biochim. Biophys. Acta Gen. Subj.* **2021**, *1865*, 129486.
- [9] G. A. Shamsan, D. J. Odde, *Curr. Opin. Chem. Biol.* **2019**, *53*, 125–130.
- [10] R. Jöhr, M. S. Bauer, L. C. Schendel, C. Kluger, H. E. Gaub, *Nano Lett.* **2019**, *19*, 3176–3181.
- [11] E. M. Gates, A. S. LaCroix, K. E. Rothenberg, B. D. Hoffman, *Cytometry Part A* **2019**, *95*, 201–213.
- [12] E. Sitarska, A. Diz-Muñoz, *Curr. Opin. Cell Biol.* **2020**, *66*, 11–18.
- [13] M. Krieg, G. Fläschner, D. Alsteens, B. M. Gaub, W. H. Roos, G. J. L. Wuite, H. E. Gaub, C. Gerber, Y. F. Dufrêne, D. J. Müller, *Nat. Rev. Phys.* **2019**, *1*, 41–57.
- [14] P. Roca-Cusachs, V. Conte, X. Trepat, *Nat. Cell Biol.* **2017**, *19*, 742–751.
- [15] A. Diz-Muñoz, O. D. Weiner, D. A. Fletcher, *Nat. Phys.* **2018**, *14*, 648–652.
- [16] C. Grashoff, B. D. Hoffman, M. D. Brenner, R. Zhou, M. Parsons, M. T. Yang, M. A. McLean, S. G. Sligar, C. S. Chen, T. Ha, M. A. Schwartz, *Nature* **2010**, *466*, 263–266.
- [17] B. Baumeister, S. Matile, *Chem. Eur. J.* **2000**, *6*, 1739–1749.
- [18] S. Begum, M. Cianci, B. Durbeel, O. Falklöf, A. Hädener, J. R. Helliwell, M. Helliwell, A. C. Regan, C. I. F. Watt, *Phys. Chem. Chem. Phys.* **2015**, *17*, 16723–16732.
- [19] A. P. Gamiz-Hernandez, I. N. Angelova, R. Send, D. Sundholm, V. R. I. Kaila, *Angew. Chem. Int. Ed.* **2015**, *54*, 11564–11566; *Angew. Chem.* **2015**, *127*, 11726–11729.
- [20] L. Assies, J. García-Calvo, F. Piazzolla, S. Sanchez, T. Kato, L. Reymond, A. Goujon, A. Colom, J. López-Andarias, K. Straková, D. Mahecic, V. Mercier, M. Riggi, N. Jiménez-Rojo, C. Roffay, G. Licari, M. Tsemperouli, F. Neuhaus, A. Fürstenberg, E. Vauthey, S. Hoogendoorn, M. Gonzalez-Gaitan, A. Zumbuehl, K. Sugihara, J. Gruenberg, H. Riezman, R. Loewith, S. Manley, A. Roux, N. Winssinger, N. Sakai, S. Pitsch, S. Matile, *Chimia* **2021**, *75*, 1004–1011.
- [21] T. Kato, K. Strakova, J. García-Calvo, N. Sakai, S. Matile, *Bull. Chem. Soc. Jpn.* **2020**, *93*, 1401–1411.
- [22] K. Strakova, L. Assies, A. Goujon, F. Piazzolla, H. V. Humeniuk, S. Matile, *Chem. Rev.* **2019**, *119*, 10977–11005.
- [23] M. Riggi, *TheScienceBreaker* **2022**, <https://doi.org/10.25250/thescbr.brk611>.
- [24] M. Sheves, K. Nakanishi, B. Honig, *J. Am. Chem. Soc.* **1979**, *101*, 7086–7088.
- [25] P. D. Kiser, M. Golczak, K. Palczewski, *Chem. Rev.* **2014**, *114*, 194–232.
- [26] J.-Y. Winum, S. Matile, *J. Am. Chem. Soc.* **1999**, *121*, 7961–7962.
- [27] N. Sakai, D. Houdebert, S. Matile, *Chem. Eur. J.* **2003**, *9*, 223–232.

- [28] A. Fin, A. Vargas Jentzsch, N. Sakai, S. Matile, *Angew. Chem. Int. Ed.* **2012**, *51*, 12736–12739; *Angew. Chem.* **2012**, *124*, 12908–12911.
- [29] H. Hayashi, A. Sobczuk, A. Bolag, N. Sakai, S. Matile, *Chem. Sci.* **2014**, *5*, 4610–4614.
- [30] M. Dal Molin, Q. Verolet, A. Colom, R. Letrun, E. Derivery, M. Gonzalez-Gaitan, E. Vauthey, A. Roux, N. Sakai, S. Matile, *J. Am. Chem. Soc.* **2015**, *137*, 568–571.
- [31] S. Soleimanpour, A. Colom, E. Derivery, M. Gonzalez-Gaitan, A. Roux, N. Sakai, S. Matile, *Chem. Commun.* **2016**, *52*, 14450–14453.
- [32] N. Chuard, K. Fujisawa, P. Morelli, J. Saarbach, N. Winsinger, P. Metrangolo, G. Resnati, N. Sakai, S. Matile, *J. Am. Chem. Soc.* **2016**, *138*, 11264–11271.
- [33] A. Colom, E. Derivery, S. Soleimanpour, C. Tomba, M. D. Molin, N. Sakai, M. González-Gaitán, S. Matile, A. Roux, *Nat. Chem.* **2018**, *10*, 1118–1125.
- [34] M. Macchione, A. Goujon, K. Strakova, H. V. Humeniuk, G. Licari, E. Tajkhorshid, N. Sakai, S. Matile, *Angew. Chem. Int. Ed.* **2019**, *58*, 15752–15756; *Angew. Chem.* **2019**, *131*, 15899–15903.
- [35] J. García-Calvo, J. Maillard, I. Furera, K. Strakova, A. Colom, V. Mercier, A. Roux, E. Vauthey, N. Sakai, A. Fürstenberg, S. Matile, *J. Am. Chem. Soc.* **2020**, *142*, 12034–12038.
- [36] J. García-Calvo, J. López-Andarias, J. Maillard, V. Mercier, C. Roffay, A. Roux, A. Fürstenberg, N. Sakai, S. Matile, *Chem. Sci.* **2022**, *13*, 2086–2093.
- [37] J. Frey, A. D. Bond, A. B. Holmes, *Chem. Commun.* **2002**, 2424–2425.
- [38] G. Barbarella, L. Favaretto, G. Sotgiu, L. Antolini, G. Gigli, R. Cingolani, A. Bongini, *Chem. Mater.* **2001**, *13*, 4112–4122.
- [39] T. Ozturk, E. Ertas, O. Mert, *Tetrahedron* **2005**, *61*, 11055–11077.
- [40] A. Mishra, C.-Q. Ma, P. Bäuerle, *Chem. Rev.* **2009**, *109*, 1141–1276.
- [41] A. Goujon, K. Straková, N. Sakai, S. Matile, *Chem. Sci.* **2019**, *10*, 310–319.
- [42] A. Bauzá, T. J. Mooibroek, A. Frontera, *ChemPhysChem* **2015**, *16*, 2496–2517.
- [43] L. Vogel, P. Wonner, S. M. Huber, *Angew. Chem. Int. Ed.* **2019**, *58*, 1880–1891; *Angew. Chem.* **2019**, *131*, 1896–1907.
- [44] P. Scilabra, G. Terraneo, G. Resnati, *Acc. Chem. Res.* **2019**, *52*, 1313–1324.
- [45] B. R. Beno, K.-S. Yeung, M. D. Bartberger, L. D. Pennington, N. A. Meanwell, *J. Med. Chem.* **2015**, *58*, 4383–4438.
- [46] S. Benz, J. López-Andarias, J. Mareda, N. Sakai, S. Matile, *Angew. Chem. Int. Ed.* **2017**, *56*, 812–815; *Angew. Chem.* **2017**, *129*, 830–833.
- [47] N. Biot, D. Bonifazi, *Coord. Chem. Rev.* **2020**, *413*, 213243.
- [48] L. E. Bickerton, A. Docker, A. J. Sterling, H. Kuhn, F. Duarte, P. D. Beer, M. J. Langton, *Chem. Eur. J.* **2021**, *27*, 11738–11745.
- [49] M. S. Taylor, *Coord. Chem. Rev.* **2020**, *413*, 213270.
- [50] M. Macchione, N. Chuard, N. Sakai, S. Matile, *ChemPlusChem* **2017**, *82*, 1062–1066.
- [51] J. García-Calvo, J. López-Andarias, N. Sakai, S. Matile, *Chem. Commun.* **2021**, *57*, 3913–3916.
- [52] J. García-Calvo, J. López-Andarias, N. Sakai, S. Matile, *Helv. Chim. Acta* **2022**, *105*, e202100238.
- [53] Q. Verolet, A. Rosspeintner, S. Soleimanpour, N. Sakai, E. Vauthey, S. Matile, *J. Am. Chem. Soc.* **2015**, *137*, 15644–15647.
- [54] K. Strakova, A. I. Poblador-Bahamonde, N. Sakai, S. Matile, *Chem. Eur. J.* **2019**, *25*, 14935–14942.
- [55] G. Licari, K. Strakova, S. Matile, E. Tajkhorshid, *Chem. Sci.* **2020**, *11*, 5637–5649.
- [56] F. Neuhaus, F. Zobi, G. Brezesinski, M. Dal Molin, S. Matile, A. Zumbuehl, *Beilstein J. Org. Chem.* **2017**, *13*, 1099–1105.
- [57] J. López-Andarias, K. Straková, R. Martinent, N. Jiménez-Rojo, H. Riezman, N. Sakai, S. Matile, *JACS Au* **2021**, *1*, 221–232.
- [58] J. López-Andarias, K. Eblighatian, Q. T. L. Pasquer, L. Assies, N. Sakai, S. Hoogendoorn, S. Matile, *Angew. Chem. Int. Ed.* **2022**, *61*, e202113163; *Angew. Chem.* **2022**, *134*, e202113163.
- [59] N. Sakai, L. Assies, S. Matile, *Helv. Chim. Acta* **2022**, *105*, e202200052.
- [60] C. Zhong, *Phys. Chem. Chem. Phys.* **2015**, *17*, 9248–9257.
- [61] K. Oglecka, P. Rangamani, B. Liedberg, R. S. Kraut, A. N. Parikh, *eLife* **2014**, *3*, e03695.
- [62] J. C. S. Ho, P. Rangamani, B. Liedberg, A. N. Parikh, *Langmuir* **2016**, *32*, 2151–2163.
- [63] T. Hamada, Y. Kishimoto, T. Nagasaki, M. Takagi, *Soft Matter* **2011**, *7*, 9061–9068.
- [64] A. Goujon, A. Colom, K. Straková, V. Mercier, D. Mahecic, S. Manley, N. Sakai, A. Roux, S. Matile, *J. Am. Chem. Soc.* **2019**, *141*, 3380–3384.
- [65] K. Straková, J. López-Andarias, N. Jiménez-Rojo, J. E. Chambers, S. J. Marciak, H. Riezman, N. Sakai, S. Matile, *ACS Cent. Sci.* **2020**, *6*, 1376–1385.
- [66] D. Mahecic, L. Carlini, T. Kleele, A. Colom, A. Goujon, S. Matile, A. Roux, S. Manley, *Cell Rep.* **2021**, *35*, 108947.
- [67] C. Roffay, J. M. G. Arcos, P. Chapuis, J. López-Andarias, A. Colom, C. Tomba, I. D. Meglio, S. Matile, A. Roux, V. Mercier, *bioRxiv* **2022**, <https://doi.org/10.1101/2022.09.28.509885>.
- [68] J. Liu, Z. Cui, *Bioconjugate Chem.* **2020**, *31*, 1587–1595.
- [69] P. Gao, W. Pan, N. Li, B. Tang, *Chem. Sci.* **2019**, *10*, 6035–6071.
- [70] N. Trinh, K. A. Jolliffe, E. J. New, *Angew. Chem. Int. Ed.* **2020**, *59*, 20290–20301; *Angew. Chem.* **2020**, *132*, 20466–20479.
- [71] N. Wagner, M. Stephan, D. Höglinder, A. Nadler, *Angew. Chem. Int. Ed.* **2018**, *57*, 13339–13343; *Angew. Chem.* **2018**, *130*, 13523–13527.
- [72] F. Piazzolla, V. Mercier, L. Assies, N. Sakai, A. Roux, S. Matile, *Angew. Chem. Int. Ed.* **2021**, *60*, 12258–12263; *Angew. Chem.* **2021**, *133*, 12366–12371.
- [73] L. Assies, V. Mercier, J. López-Andarias, A. Roux, N. Sakai, S. Matile, *ChemBioChem* **2022**, *23*, e202200192.
- [74] B. Baumeister, A. Som, G. Das, N. Sakai, F. Vilbois, D. Gerard, S. P. Shahi, S. Matile, *Helv. Chim. Acta* **2002**, *85*, 2740–2753.
- [75] D. Bashford, M. Karplus, *J. Phys. Chem.* **1991**, *95*, 9556–9561.
- [76] Z. Yue, C. Li, G. A. Voth, J. M. J. Swanson, *J. Am. Chem. Soc.* **2019**, *141*, 13421–13433.
- [77] C. A. Fitch, G. Platzer, M. Okon, B. Garcia-Moreno E, L. P. McIntosh, *Protein Sci.* **2015**, *24*, 752–761.
- [78] M. I. Niemeyer, F. D. González-Nilo, L. Zúñiga, W. González, L. P. Cid, F. V. Sepúlveda, *Proc. Natl. Acad. Sci. USA* **2007**, *104*, 666–671.
- [79] A. Jiménez-Sánchez, E. K. Lei, S. O. Kelley, *Angew. Chem. Int. Ed.* **2018**, *57*, 8891–8895; *Angew. Chem.* **2018**, *130*, 9029–9033.
- [80] G. Boncompain, S. Divoux, N. Gareil, H. de Forges, A. Lescure, L. Latreche, V. Mercanti, F. Jollivet, G. Raposo, F. Perez, *Nat. Methods* **2012**, *9*, 493–498.
- [81] G. C. R. Ellis-Davies, *Acc. Chem. Res.* **2020**, *53*, 1593–1604.
- [82] J. H. Lorent, K. R. Levental, L. Ganesan, G. Rivera-Longsworth, E. Sezgin, M. Doktorova, E. Lyman, I. Levental, *Nat. Chem. Biol.* **2020**, *16*, 644–652.
- [83] B. W. Hoogenboom, L. E. Hough, E. A. Lemke, R. Y. H. Lim, P. R. Onck, A. Zilman, *Phys. Rep.* **2021**, *921*, 1–53, <https://doi.org/10.1016/j.physrep.2021.03.003>.

- [84] N. Zuleger, M. I. Robson, E. C. Schirmer, *Nucleus* **2011**, *2*, 339–349.
- [85] E. Mertz, S. C. Zimmerman, *J. Am. Chem. Soc.* **2003**, *125*, 3424–3425.
- [86] Y. Xu, S. Yu, Y. Wang, L. Hu, F. Zhao, X. Chen, Y. Li, X. Yu, L. Pu, *Eur. J. Org. Chem.* **2016**, 5868–5875.
- [87] D. I. Danylchuk, S. Moon, K. Xu, A. S. Klymchenko, *Angew. Chem. Int. Ed.* **2019**, *58*, 14920–14924; *Angew. Chem.* **2019**, *131*, 15062–15066.
- [88] N. Oleksiievets, Y. Sargsyan, J. C. Thiele, N. Mougios, S. Sograte-Idrissi, O. Nevskyi, I. Gregor, F. Opazo, S. Thoms, J. Enderlein, R. Tsukanov, *Commun. Biol.* **2022**, *5*, 38.
- [89] D. Lachowski, C. Matellan, S. Gopal, E. Cortes, B. K. Robinson, A. Saiani, A. F. Miller, M. M. Stevens, A. E. del Río Hernández, *ACS Nano* **2022**, *16*, 4322–4337.
- [90] C. Tomba, V. Luchnikov, L. Barberi, C. Blanch-Mercader, A. Roux, *Dev. Cell* **2022**, *57*, 1257–1270.
- [91] J. Park, S. Jia, D. Salter, P. Bagnaninchi, C. G. Hansen, *EMBO J.* **2022**, *41*, e108719.
- [92] S. Wang, B. Wang, Y. Shi, T. Möller, R. I. Stegmeyer, B. Strilic, T. Li, Z. Yuan, C. Wang, N. Wettschureck, D. Vestweber, S. Offermanns, *Blood* **2022**, *140*, 171–183.
- [93] X. Chen, X. Song, J. Li, R. Zhang, C. Yu, Z. Zhou, J. Liu, S. Liao, D. J. Klionsky, G. Kroemer, J. Liu, D. Tang, R. Kang, *Autophagy* **2022**, 74–94.
- [94] M. Wang, C. Xiong, A. M. Mercurio, *J. Cell Biol.* **2022**, *221*, e202108083.
- [95] S. Mylvaganam, J. Plumb, B. Yusuf, R. Li, C.-Y. Lu, L. A. Robinson, S. A. Freeman, S. Grinstein, *Nat. Cell Biol.* **2022**, *24*, 1226–1238.
- [96] C. Royer, E. Sandham, E. Slee, F. Schneider, C. B. Lagerholm, J. Godwin, N. Veits, H. Hathrell, F. Zhou, K. Leonavicius, J. Garratt, T. Narendra, A. Vincent, C. Jones, T. Child, K. Coward, C. Graham, M. Fritzsche, X. Lu, S. Srinivas, *Nat. Commun.* **2022**, *13*, 941.
- [97] K. Bera, A. Kiepas, I. Godet, Y. Li, P. Mehta, B. Ifemembi, C. D. Paul, A. Sen, S. A. Serra, K. Stoletov, J. Tao, G. Shatkin, S. J. Lee, Y. Zhang, A. Boen, P. Mistriotis, D. M. Gilkes, J. D. Lewis, C.-M. Fan, A. P. Feinberg, M. A. Valverde, S. X. Sun, K. Konstantopoulos, *Nature* **2022**, *611*, 365–373.
- [98] Z. Shen, K. T. Belcheva, M. Jelcic, K. L. Hui, A. Katikaneni, P. Niethammer, *Proc. Natl. Acad. Sci. USA* **2022**, *119*, e2112390119.
- [99] A. Saha, S. Mandal, J. V. V. Arafiles, J. Gómez-González, C. P. R. Hackenberger, A. Brik, *Angew. Chem. Int. Ed.* **2022**, *61*, e202207551; *Angew. Chem.* **2022**, *134*, e202207551.
- [100] S. Maassen, H. Warner, M. Ioannidis, J. Jansma, H. Markus, S. El Aidy, M.-D. Chiara, J. L. Chiara, L. Maierhofer, H. Weavers, G. van den Bogaart, *Free Radical Biol. Med.* **2022**, *188*, 287–297.
- [101] A. Atmanli, A. C. Chai, M. Cui, Z. Wang, T. Nishiyama, R. Bassel-Duby, E. N. Olson, *Circ. Res.* **2021**, *129*, 602–616.
- [102] S. Blonski, J. Aureille, S. Badawi, D. Zaremba, L. Pernet, A. Grichine, S. Fraboulet, P. M. Korczyk, P. Recho, C. Guilluy, M. E. Dolega, *Dev. Cell* **2021**, *56*, 3222–3234.
- [103] A. Claude-Taupin, J. Jia, Z. Bhujabal, M. Garfa-Traoré, S. Kumar, G. P. D. da Silva, R. Javed, Y. Gu, L. Allers, R. Peters, F. Wang, L. J. da Costa, S. Pallikkuth, K. A. Lidke, M. Mauthe, P. Verlhac, Y. Uchiyama, M. Salemi, B. Phinney, S. A. Tooze, M. C. Mari, T. Johansen, F. Reggiori, V. Deretic, *Nat. Cell Biol.* **2021**, *23*, 846–858.
- [104] S. Gupta, J. Yano, V. Mercier, H. H. Htwe, H. R. Shin, G. Rademaker, Z. Cakir, T. Ituarte, K. W. Wen, G. E. Kim, R. Zoncu, A. Roux, D. W. Dawson, R. M. Perera, *Nat. Cell Biol.* **2021**, *23*, 232–242.
- [105] A. F. L. Schneider, M. Kithil, M. C. Cardoso, M. Lehmann, C. P. R. Hackenberger, *Nat. Chem.* **2021**, *13*, 530–539.
- [106] C. Roffay, G. Molinard, K. Kim, M. Urbanska, V. Andrade, V. Barbarasa, P. Nowak, V. Mercier, J. García-Calvo, S. Matile, R. Loewith, A. Echard, J. Guck, M. Lenz, A. Roux, *Proc. Natl. Acad. Sci. USA* **2021**, *118*, e2103228118.
- [107] V. Mercier, J. Larios, G. Molinard, A. Goujon, S. Matile, J. Gruenberg, A. Roux, *Nat. Cell Biol.* **2020**, *22*, 947–959.
- [108] T. Sansen, D. Sanchez-Fuentes, R. Rathar, A. Colom-Diego, F. El Alaoui, J. Viaud, M. Macchione, S. de Rossi, S. Matile, R. Gaudin, V. Bäcker, A. Carretero-Genevrier, L. Picas, *ACS Appl. Mater. Interfaces* **2020**, *12*, 29000–29012.
- [109] S. W. Wong, S. Lenzini, R. Bargi, Z. Feng, C. Macaraniag, J. C. Lee, Z. Peng, J. Shin, *Adv. Sci.* **2020**, *7*, 2001066.
- [110] M. M. Nava, Y. A. Miroshnikova, L. C. Biggs, D. B. Whitefield, F. Metge, J. Boucas, H. Vihinen, E. Jokitalo, X. Li, J. M. García Arcos, B. Hoffmann, R. Merkel, C. M. Niessen, K. N. Dahl, S. A. Wickström, *Cell* **2020**, *181*, 800–817.
- [111] L. Oberhauser, S. Granziera, A. Colom, A. Goujon, V. Lavallard, S. Matile, A. Roux, T. Brun, P. Maechler, *Biochim. Biophys. Acta Mol. Cell Res.* **2020**, *1867*, 118619.
- [112] J. Wang, W. Tan, G. Li, D. Wu, H. He, J. Xu, M. Yi, Y. Zhang, S. A. Aghvami, S. Fraden, B. Xu, *Chem. Eur. J.* **2020**, *26*, 15116–15120.
- [113] N. Jiménez-Rojo, M. D. Leonetti, V. Zoni, A. Colom, S. Feng, N. R. Iyengar, S. Matile, A. Roux, S. Vanni, J. S. Weissman, H. Riezman, *Curr. Biol.* **2020**, *30*, 3775–3787.
- [114] J. H. R. Hetmanski, H. de Belly, I. Busnelli, T. Waring, R. V. Nair, V. Sokleva, O. Dobre, A. Cameron, N. Gauthier, C. Lamaze, J. Swift, A. del Campo, T. Starborg, T. Zech, J. G. Goetz, E. K. Paluch, J.-M. Schwartz, P. T. Caswell, *Dev. Cell* **2019**, *51*, 460–475.
- [115] M. Riggi, C. Bourgoint, M. Macchione, S. Matile, R. Loewith, A. Roux, *J. Biol. Chem.* **2019**, *218*, 2265–2276.
- [116] M. Riggi, K. Niewola-Staszkowska, N. Chiaruttini, A. Colom, B. Kusmider, V. Mercier, S. Soleimanpour, M. Stahl, S. Matile, A. Roux, R. Loewith, *Nat. Cell Biol.* **2018**, *20*, 1043–1051.
- [117] S. Wang, S. Cao, M. Arhatte, D. Li, Y. Shi, S. Kurz, J. Hu, L. Wang, J. Shao, A. Atzberger, Z. Wang, C. Wang, W. Zang, I. Fleming, N. Wettschureck, E. Honoré, S. Offermanns, *Nat. Commun.* **2020**, *11*, 2303.
- [118] K. Rahman, C. A. Coomer, S. Majdoul, S. Y. Ding, S. Padilla-Parra, A. A. Compton, *eLife* **2020**, *9*, e58537.
- [119] Leica Microsystems, “Understanding the Basis for Morphogenesis in the Early Mammalian Embryo,” **2022**, July 7, <https://twitter.com/LeicaMicro/status/1545029875077001220>.
- [120] A. S. Klymchenko, *Acc. Chem. Res.* **2017**, *50*, 366–375.
- [121] I. López-Duarte, T. T. Vu, M. A. Izquierdo, J. A. Bull, M. K. Kuimova, *Chem. Commun.* **2014**, *50*, 5282–5284.
- [122] A. Vyšniauskas, M. Balaz, H. L. Anderson, M. K. Kuimova, *Phys. Chem. Chem. Phys.* **2015**, *17*, 7548–7554.
- [123] J. E. Chambers, M. Kubánková, R. G. Huber, I. López-Duarte, E. Avezov, P. J. Bond, S. J. Marciniak, M. K. Kuimova, *ACS Nano* **2018**, *12*, 4398–4407.
- [124] J. A. Robson, M. Kubánková, T. Bond, R. A. Hendley, A. J. P. White, M. K. Kuimova, J. D. E. T. Wilton-Ely, *Angew. Chem. Int. Ed.* **2020**, *59*, 21431–21435; *Angew. Chem.* **2020**, *132*, 21615–21619.
- [125] X. Peng, Z. Yang, J. Wang, J. Fan, Y. He, F. Song, B. Wang, S. Sun, J. Qu, J. Qi, M. Yan, *J. Am. Chem. Soc.* **2011**, *133*, 6626–6635.
- [126] L. Wang, Y. Xiao, W. Tian, L. Deng, *J. Am. Chem. Soc.* **2013**, *135*, 2903–2906.
- [127] Z. Yang, Y. He, J.-H. Lee, N. Park, M. Suh, W.-S. Chae, J. Cao, X. Peng, H. Jung, C. Kang, J. S. Kim, *J. Am. Chem. Soc.* **2013**, *135*, 9181–9185.

- [128] Z. Yang, D. H. Kang, H. Lee, J. Shin, W. Yan, B. Rathore, H.-R. Kim, S. J. Kim, H. Singh, L. Liu, J. Qu, C. Kang, J. S. Kim, *Bioconjugate Chem.* **2018**, *29*, 1446–1453.
- [129] I. E. Steinmark, A. L. James, P.-H. Chung, P. E. Morton, M. Parsons, C. A. Dreiss, C. D. Lorenz, G. Yahiroglu, K. Suhling, *PLoS One* **2019**, *14*, e0211165.
- [130] Y. Zheng, Y. Ding, J. Ren, Y. Xiang, Z. Shuai, A. Tong, *Anal. Chem.* **2020**, *92*, 14494–14500.
- [131] Y. Zheng, Y. Ding, X. Zheng, C. Zhang, Y. Zhang, Y. Xiang, A. Tong, *Anal. Chem.* **2021**, *93*, 10272–10281.
- [132] Y. Zhao, H. S. Kim, X. Zou, L. Huang, X. Liang, Z. Li, J. S. Kim, W. Lin, *J. Am. Chem. Soc.* **2022**, *144*, 20854–20865.
- [133] Y. V. Suseela, N. Narayanaswamy, S. Pratihar, T. Govindaraju, *Chem. Soc. Rev.* **2018**, *47*, 1098–1131.
- [134] F. Würthner, *Angew. Chem. Int. Ed.* **2020**, *59*, 14192–14196; *Angew. Chem.* **2020**, *132*, 14296–14301.
- [135] T. Yamakado, S. Saito, *J. Am. Chem. Soc.* **2022**, *144*, 2804–2815.
- [136] W. Nakanishi, S. Saito, N. Sakamoto, A. Kashiwagi, S. Yamaguchi, H. Sakai, K. Ariga, *Chem. Asian J.* **2019**, *14*, 2869–2876.
- [137] R. Kimura, H. Kuramochi, P. Liu, T. Yamakado, A. Osuka, T. Tahara, S. Saito, *Angew. Chem. Int. Ed.* **2020**, *59*, 16430–16435; *Angew. Chem.* **2020**, *132*, 16572–16577.
- [138] R. Kimura, H. Kitakado, T. Yamakado, H. Yoshida, S. Saito, *Chem. Commun.* **2022**, *58*, 2128–2131.
- [139] Z. Zhang, G. Sun, W. Chen, J. Su, H. Tian, *Chem. Sci.* **2020**, *11*, 7525–7537.
- [140] H. V. Humeniuk, A. Rosspeintner, G. Licari, V. Kilin, L. Bonacina, E. Vauthey, N. Sakai, S. Matile, *Angew. Chem. Int. Ed.* **2018**, *57*, 10559–10563; *Angew. Chem.* **2018**, *130*, 10719–10723.
- [141] E. Sezgin, T. Sadowski, K. Simons, *Langmuir* **2014**, *30*, 8160–8166.
- [142] F. Effenberger, F. Würthner, *Angew. Chem. Int. Ed. Engl.* **1993**, *32*, 719–721; *Angew. Chem.* **1993**, *105*, 742–744.
- [143] R. Flores-Cruz, C. Hernández-Juárez, A. Jiménez-Sánchez, *Eur. J. Org. Chem.* **2022**, e202200626.
- [144] E. Sezgin, F. Schneider, V. Zilles, I. Urbančič, E. Garcia, D. Waithe, A. S. Klymchenko, C. Eggeling, *Biophys. J.* **2017**, *113*, 1321–1330.
- [145] D. I. Danylchuk, P.-H. Jouard, A. S. Klymchenko, *J. Am. Chem. Soc.* **2021**, *143*, 912–924.
- [146] L. Jin, A. C. Millard, J. P. Wuskell, X. Dong, D. Wu, H. A. Clark, L. M. Loew, *Biophys. J.* **2006**, *90*, 2563–2575.
- [147] D. M. Owen, P. M. P. Lanigan, C. Dunsby, I. Munro, D. Grant, M. A. A. Neil, P. M. W. French, A. I. Magee, *Biophys. J.* **2006**, *90*, L80–82.
- [148] N. Li, W. Zhang, H. Lin, J.-M. Lin, *Chin. Chem. Lett.* **2022**, *33*, 1377–1380.
- [149] M. Páez-Pérez, I. López-Duarte, A. Vyšniauskas, N. J. Brooks, M. K. Kuimova, *Chem. Sci.* **2021**, *12*, 2604–2613.
- [150] C.-H. Wu, Y. Chen, K. A. Pyrshev, Y.-T. Chen, Z. Zhang, K.-H. Chang, S. O. Yesylevskyy, A. P. Demchenko, P.-T. Chou, *ACS Chem. Biol.* **2020**, *15*, 1862–1873.
- [151] S. Sasaki, S. Suzuki, W. M. C. Sameera, K. Igawa, K. Morokuma, G. Konishi, *J. Am. Chem. Soc.* **2016**, *138*, 8194–8206.
- [152] J. Adachi, H. Oda, T. Fukushima, B. Lestari, H. Kimura, H. Sugai, K. Shiraki, K. Sato, K. Kinbara, *ChemRxiv* **2022**, <https://doi.org/10.26434/chemrxiv-2022-p8jq4>.
- [153] M. K. Kuimova, M. Balaz, H. L. Anderson, P. R. Ogilby, *J. Am. Chem. Soc.* **2009**, *131*, 7948–7949.
- [154] N. P. Kamat, Z. Liao, L. E. Moses, J. Rawson, M. J. Therien, I. J. Dmochowski, D. A. Hammer, *Proc. Natl. Acad. Sci. USA* **2011**, *108*, 13984–13989.
- [155] T. Muraoka, K. Umetsu, K. V. Tabata, T. Hamada, H. Noji, T. Yamashita, K. Kinbara, *J. Am. Chem. Soc.* **2017**, *139*, 18016–18023.
- [156] K. Sato, T. Muraoka, K. Kinbara, *Acc. Chem. Res.* **2021**, *54*, 3700–3709.
- [157] N. Sakai, S. Matile, *J. Am. Chem. Soc.* **2018**, *140*, 11438–11443.
- [158] Y. Bagheri, A. A. Ali, P. Keshri, J. Chambers, A. Gershenson, M. You, *Angew. Chem. Int. Ed.* **2022**, *61*, e202112033; *Angew. Chem.* **2022**, *134*, e202112033.
- [159] A. S. Klymchenko, A. P. Demchenko, *J. Am. Chem. Soc.* **2002**, *124*, 12372–12379.
- [160] A. S. Klymchenko, S. Oncul, P. Didier, E. Schaub, L. Bagatolli, G. Duportail, Y. Mély, *Biochim. Biophys. Acta Biomembr.* **2009**, *1788*, 495–499.
- [161] P. Liu, E. W. Miller, *Acc. Chem. Res.* **2020**, *53*, 11–19.
- [162] M. Macchione, M. Tsemperouli, A. Goujon, A. R. Mallia, N. Sakai, K. Sugihara, S. Matile, *Helv. Chim. Acta* **2018**, *101*, e1800014.
- [163] C. Romero-Nieto, T. Baumgartner, *Synlett* **2013**, *24*, 920–937.
- [164] C. Wang, M. Taki, K. Kajiwara, J. Wang, S. Yamaguchi, *ACS Mater. Lett.* **2020**, *2*, 705–711.
- [165] Q. Verolet, S. Soleimanpour, K. Fujisawa, M. Dal Molin, N. Sakai, S. Matile, *ChemistryOpen* **2015**, *4*, 264–267.
- [166] X. Zhang, N. Sakai, S. Matile, *ChemistryOpen* **2020**, *9*, 18–22.
- [167] M. Tasior, O. Vakuliuk, D. Koga, B. Koszarna, K. Górska, M. Grzybowski, Ł. Kieleski, M. Krzeszewski, D. T. Gryko, *J. Org. Chem.* **2020**, *85*, 13529–13543.

Manuscript received: December 9, 2022

Accepted manuscript online: February 3, 2023

Version of record online: February 23, 2023